Title
TRIP PHENOMENA IN IMPACT TESTS.

Author
Dokko, Chung.

Publication Date
1969-09-01

UCRL-19068

cy. 2

TRIP PHENOMENA IN IMPACT TESTS

Chung Dokko
(M. S. Thesis)

September 1969

AEC Contract No. W-7405-eng-48

LAWRENCE RADIATION LABORATORY
UNIVERSITY of CALIFORNIA BERKELEY

cy. 2

UCRL-19068

DISCLAIMER

TABLE OF CONTENTS

TRIP PHENOMENA IN IMPACT TESTS

Chung Dokko

Inorganic Materials Research Division, Lawrence Radiation Laboratory,
Department of Materials Science and Engineering, College of Engineering
University of California, Berkeley, California

ABSTRACT

This investigation is concerned with the fracture toughness of high-strength steels which exhibit the strain-induced martensite transformation during the test, providing a good combination of strength and ductility.

Since the temperature rise due to high loading rates could possibly suppress the transformation when the M_D temperature is exceeded, Charpy impact tests were used in order to achieve a nearly adiabatic condition.

Slow bend tests were also conducted to study the loading rate effects. The change in the loading rate from the Charpy impact to the slow bend test did not cause a recognizable enhancement of the martensite formation but rather a reduced plastic zone size was observed for the slow bend tests.

The fracture toughness, defined by the Charpy energy divided by the fracture area, was studied as a function of carbon content, rolling temperature, amount of prior deformation and test temperature.

Energy absorption during crack propagation was controlled by the plastic energy dissipation per unit volume and by the total contributing volume.

The steel with the lower yield strength and strain hardening rate in the tensile tests produced a larger plastic zone size as tested in the Charpy impact tests. At the same yield strength level, fracture

toughness decreased linearly with the increase in strain hardening rate obtained from tensile test for all test temperatures.

An exponentially inverse relationship was found between toughness and tensile strength.

I. INTRODUCTION

The combination of high strength and high fracture toughness is quite often difficult to achieve. While the strength can be obtained by limiting dislocation mobility, the freedom from sudden or catastropic failure involves stopping crack advancement by plastic flow.

Among the many variables associated with plastic deformation, ductility is usually considered to be the best safeguard for preventing failure. High ductility is normal for low strength materials. It was shown, however, that elongation and reduction of area measurements may have little correlation with fracture toughness, since the propagation of a crack can be controlled by localized variations in the microstructure such as the presence of a tough second phase.[1,2]

The TRIP (TRansformation Induced Plasticity) steels are known to increase the rate of change of energy absorption by the strain-induced martensite transformation while retaining strength and ductility (i.e., uniform elongation).

In uniaxial tensile tests, the beneficial effect of the strain-induced martensite is its inhibition of the localized plastic flow around the region where necking would otherwise have taken place at a high level of plastic strain by serving as strong barriers to dislocation motion.

Gerberich et al.[3] were led to the tentative conclusion that such a mechanism may be a primary energy absorbing medium, about 5 times as effective as those plastic dissipation processes normally occurring at a crack tip.

The same investigators also observed that there appeared to be a

definite decrease in notch toughness with increasing crosshead speed, suggesting that the transformation could possibly be suppressed at higher strain rates because of adiabatic heating.

The present investigation was prompted by this earlier work. The Charpy impact test was of particular interest because of very high strain rate ($>10^2$) involved therein. The objective for this work was to study the temperature rise effects on the strain-induced martensite transformation, as well as other factors affecting the fracture toughness.

II. EXPERIMENTAL PROCEDURE

A. Material Preparation

Chemical composition of the alloys is as follows:

Ingot No.	Cr	Ni	Mn	Si	Mo	V	N	C	Fe
675-3	9	8	2.4	1.9	1	0.57	0.09	0.2	balance
675-4	9	8	2.4	1.9	1	0.95	0.08	0.3	balance

The alloys were prepared by induction melting in a nitrogen atmosphere and addition of a high nitrogen-iron alloy. After forging, the ingot was austenitized 1 hour at 1100°C and then cut into smaller pieces. Five pieces were hot rolled at 900°C to each intermediate thicknesses in order to produce different amounts of reduction: 20, 60, 80 and 90% by final rolling at 250° and 450°C to the thickness of 0.050 inches. After rolling the specimens were air-cooled to room temperature.

Tensile and subsized Charpy impact test specimens were ground from the 0.050 inch thick sheet. All Charpy specimens except eight 0.2%C specimens were cut so that the length was perpendicular to the rolling direction (i.e. "transverse"). The tensile specimens and the eight 0.2% C Charpy specimens were cut parallel to the rolling direction (i.e. "longitudinal"). Their dimensions are shown in Figs. 1 and 2. The specimens were polished, with the removal of 0.002 inches from each surface, in order to eliminate the possible effects of surface decarburization or roll chill.

B. Mechanical Tests

1. Tensile Tests

Two Instron testing machines were used at different crosshead speeds:

0.04, 0.4, 5, and 20 in/min. for 675-3 alloy

0.04 in/min. only for 675-4 alloy

Tests were run at the following temperatures: -196°C (liquid nitrogen), -80°C (dry ice), 22°C (room temperature), 100°C (boiling water), and 200°C (oil heated by an immersion coil heater).

The upper yield point is reported as the yield strength. For those cases where no yield point was exhibited, the 0.2% offset yield is reported.

For tests at other than room temperature, the continuous loading was interrupted at every 5 (or 2.5) percent elongation in order to perform magnetic measurements at room temperature. The aging effects due to taking the specimen out of the low temperature bath was slight but unavoidable. This was done because all media except liquid nitrogen were electrically conducting and the magnet coil could not be immersed in them.

In using a very high crosshead speed such as 20 in/min., some delay in the chart recording system was noticed. Overshooting instead of yield point drop was recorded at the highest speed. After failure, the necked region was photographed from two perpendicular directions using a low power microscope to make measurements of the projected fracture area.

True stress (σ_T) and true strain (ε_T) were calculated according to

the relation

$$\sigma_T = \frac{P}{A_o}(1 + \varepsilon) \tag{1}$$

$$\varepsilon_T = \log (1 + \varepsilon) \tag{2}$$

where P is the load, A_o the original cross section area, and ε the engineering strain obtained from extension divided by the original gage length. True fracture stress (σ_f) and true fracture strain (ε_f) were obtained by using

$$\sigma_f = \frac{P_f}{A_f} \tag{3}$$

$$\varepsilon_f = \log \frac{A_o}{A_f} \tag{4}$$

where P_f and A_f are the load and the cross section area at the fracture, respectively. The area under the true stress-true strain curve was integrated using a planimeter in order to obtain the energy of deformation per unit volume.

The strain hardening exponent (n) corresponding to the expression

$$\sigma_T = A\varepsilon_T^{\,n} \tag{5}$$

was determined from the slope of a log-log plot of true stress vs true strain. The strain hardening rate ($\partial\sigma_T/\partial\epsilon_T$) for the region that follows the Lüders band propagation was also determined.

2. Charpy Impact Tests

In order to eliminate gross plastic deformation before crack initiation, subsized Charpy specimens were fatigue precracked by reversed cantilever bending. A motor-driven wheel was used in contact with the specimen surface around its edge producing repeated sideway slip as well. The notch length was extended by about 0.13 inches. The depth of the fatigue crack was controlled to be substantially identical

on both surfaces, and the two surface traces appeared to be on the same macroscopic plane. Because the specimens were very thin, an essentially plane stress condition existed. During precracking, some martensite formed along the crack. Evidence of this is visible in Fig. 21. A Charpy machine with a maximum capacity of 2 ft-lb. was used. The maximum velocity of the pendulum was 11.3 ft/sec. All specimens were broken by a single blow. The Charpy impact energy was corrected for the friction and windage losses and divided by the fracture area (W/A), the fracture area being the specimen area minus the notched and fatigue cracked areas.

For other than room temperature tests, after transferring the specimen from the liquid bath, the liquid medium from the same bath was sprayed over the specimen in order to maintain the specimen temperature until the pendulum was released. The test temperatures were -196°, -80°, -30°, 22°, 100°, and 200°C.

3. Slow Bend Tests

The 675-4 alloy with the same geometry as in Charpy tests was bent slowly in the Instron machine at a crosshead speed of 0.04 in/min., using a compression cell and a three point bending fixture whose geometry essentially duplicated that of the tup and anvils of the Charpy machine. The fixture was prepared so as to keep the thin Charpy specimens from being flipped over during loading. Only room temperature slow bend tests were conducted.

4. Microhardness Measurements

A microhardness tester was utilized for making hardness measurements on the surface of Charpy specimens after fracture. Hardnesses

were obtained in an equivalent Rockwell "C" scale as a function of the transverse distance from the fracture.

C. Magnetic Measurements

A permeameter with 1/2 in. air gap was used for the magnetic measurements of tensile specimens. The volume fraction of the martensite ($V_{\alpha'}$) was obtained from[4]

$$V_{\alpha'} = \frac{\Delta\phi_{SLFS} \cdot n}{2 \cdot N \cdot A \cdot n_o} \cdot \frac{100}{B_o} , \% \qquad (6)$$

where, for the technique used in the present investigation,

$\Delta\phi_{SLFS} = 0.928 \times 10^8$ maxwell

n = mV reading

N = 10,000 turns

A = area of the specimen (cm^2)

n_o = 1000 mV

and for the alloys of interest,

B_o = 16,500 gauss

For the room temperature tests, during which the specimens were not removed from the air gap, the specimen area was obtained by linear interpolation between the original and final values. Area measurements were made before the magnetic measurements in other than the room temperature tests.

In order to obtain the maximum magnetic response, the specimens were slipped into the slot and no constraints were applied to fix the position of the specimen with respect to the air gap. Magnetic measurements could not be made for the Charpy specimens because the martensite zone was so localized around the fracture area.

The volume fractions of martensite initially present prior to testing were found to be less than 5%.

D. Temperature Measurements

An insulated copper-constantan thermocouple was tackwelded to the center of the gage length of each specimen tested at a speed higher than 5 in/min. During the tests, the emf output from the thermocouple was recorded as a function of time on a rapid-response Honeywell recorder. The attempt to measure the temperature rise during impact was unsuccessful.

E. Optical Microscopy

Some metallographic inspection was made for the Charpy specimens. In order to remove the surface tilt due to plastic deformation about 0.001 in. was additionally polished off the surface after fracture. Delamination was observed. An etchant consisting of 5 grams cupric chloride in 100 cc each of water, hydrochloric acid and methyl alcohol was used.

III. RESULTS AND DISCUSSION

A. Tensile Properties at Normal Rate (Crosshead Speed = 0.04 in/min.)

The M_s temperature was found to be below -196°C for both alloys. At 200°C, all specimens failed by early necking. The M_D temperature (above which no strain-induced martensite can be formed) increased not only with decreasing original carbon content, but also with increasing amount and temperature of prior deformation. However, for specimens highly deformed during rolling (greater than 80%), the M_D temperature was estimated to be about 140° and 120°C for 0.2%C and 0.3%C alloys respectively.

Tensile properties of the alloys at different test temperatures are listed in Table I. In general, the maximum ductility was obtained for the lowest amount of prior deformation which also produced the lowest yield strength. The yield strength increased approximately linearly with the amount of prior deformation, the slope being greater for the specimens rolled at 250°C than at 450°C.

It is shown that the yield strength was higher for the specimens rolled at 450°C with less than 60% prior deformation. With greater deformation the situation was reversed. Since the dislocation density is an important contributing factor to the strength, particularly for the highly deformed specimens during rolling, the greater slope for the lower rolling temperature suggests that there might have been less reduction of dislocation density at that temperature.

The carbide precipitation during rolling lowers the carbon content in the matrix and this presumably raises the M_D temperature. Hence, referring to Table I, it can be seen that this may be responsible for

the higher tensile strength of the specimens rolled at 450°C and the greater amount of martensite measured at the end of the test (except for 20% prior deformation). It also can be seen that for over 20% prior deformation, 0.3% C alloys have higher yield strength and tensile strength than 0.2% C alloys throughout a whole range of test temperatures, except -196°C, at which premature failures were observed.

In general, increase in strength and decrease in ductility with lowering test temperature was observed. In Table VIII, it is indicated that strain hardening rate $(\partial\sigma_T/\partial\epsilon_T)$ also increases with decreasing test temperatures.

The increasing instability toward martensite transformation with lowering test temperatures is depicted in Table II in terms of "m" and "p" or "m'". The amount of martensite can be related to the strain by the equation[5]

$$V_{\alpha'} = m\epsilon^p \qquad (7)$$

$$\text{or } V_{\alpha'} = m'\epsilon^{1/2} \qquad (8)$$

The values of "m", "p" and "m'" can be determined from the plot of $V_{\alpha'}$ vs $\epsilon^{1/2}$ on a log-log scale (Fig. 4). Namely, the value "m" is given by $V_{\alpha'}$ at $\epsilon = 1$ and "p" by half the slope because, rewriting Eq. 7

$$\log V_{\alpha'} = \log m + 2p \log \epsilon^{1/2} \qquad (9)$$

Neglecting the data points for earlier stages of straining (because the measuring technique included some of the untransformed region within the air gap), the points for each heat seem to fit a straight line. As shown in Table II, the values of "m" and "p" decreased with the increasing amount of prior deformation.

It will be noted that "p" values are, in general, different from 1/2, the discrepancy being the greatest for the specimen with 20% prior deformation tested at room temperature.

Eq. 8 seems to be valid only for low test temperatures such as -196°C, although the "m" values are listed for all test temperatures.

It is shown to be consistent that higher "m'" values are obtained for the higher rolling temperature. This means that the specimens rolled at 450°C rather than at 250°C are more prone to the strain-induced martensite transformation because of the higher M_D temperature and this can explain why the former show higher values of strain-hardening than the latter [Table IV (a)].

Fig. 3 illustrates the martensite formation due to straining. For the early stages a qualitative curve is shown as a dotted line to take into account the above mentioned averaging due to the measuring technique. There seems to be an inflection point in the $V_{\alpha'}$ vs ε curve corresponding to the end of the flat region in the σ vs ε curve. $V_{\alpha'}$ at the inflection point would represent the martensite content after the passage of the Lüders band through the length of the specimen.

It has been observed that Lüders strain decreases with increasing strain hardening rate at the same yield strength level (Fig. 5). It can be seen that, for the same strain hardening rate, a greater Lüders strain is associated with a higher σ_{LYP} (= lower yield point). The strain hardening rate increased with lower test temperature as was expected from the increased susceptability to martensite transformation [Table VIII]. Except for 20% prior deformation, higher strain hardening rate values were obtained at all test temperatures for the

specimens rolled at 450°C compared with 250°C.

B. Higher Strain Rate Effects

Previous investigators[6] reported that the strain rate per se showed minor effects on martensite formation in metastable austensite stainless steels. Test speed affected the martensite reaction through its influence on the specimen temperature. In the present investigation, similar results have been obtained.

Table III (a) shows that uniform elongations were reduced at higher test speeds. It can be noted that the relative reduction in elongation was very large for materials highly deformed at a rolling temperature of 250°C. It appears that the lower yield point increases with increasing test speed.

A marked increase in lower yield point was obtained at higher strain rates for the specimen given a 20% prior deformation at 250°C. In general, the yield strength increased with increasing strain rate and decreasing temperature with the exception of the 675-4 alloy highly deformed during rolling at 450°C and subsequently tested at dry ice temperature. As the strain rate increased, the tensile strength decreased along with decreasing amounts of martensite. Again the most severe decrease was observed for the specimens given a 20% prior deformation at 250°C. This could be expected from the transformation characteristics at the lowest speed, that is, an appreciable martensite transformation was not initiated until a very large amount of straining was achieved. It should be emphasized that the strain rate effect on martensite transformation already appeared at a low speed such as 0.4 in/min. It can be recognized that the amount of martensite obtained at

the end of the test was decreased but relative susceptabilities to transformation between different thermomechanical treatments persisted at higher strain rates. Although at intermediate strain rates, the strain hardening exponent (n) seems to vary in an unpredictable manner depending on the heats, "n" was reduced at the highest test speed and the large difference of "n" between heats at the lowest speed was almost wiped out as the test speed increased [Table IV (a)].

Table IV(b) shows that Lüders strain was increased with increasing test speed. This could have been anticipated from the previous, fixed speed results which showed that the strain hardening rate had an inverse relationship with Lüders strain. It is shown in Table IV (c) that the inherent ductility in terms of true fracture strain based on the fracture area measurements is rather insensitive to the change in strain rate.

Schematic load-extension curves at different loading rates are presented in Fig. 6. Since the deformation energy is eventually converted into heat,* the temperature would increase with increasing

---

* The martensite transformation from austensite is an exothermic reaction and the possible temperature rise due to transformation was calculated. For pure iron, the heat of reaction (γ to α) is approximately -250 cal/g atom, or-4.5 cal/g. Taking the specific heat value of 0.11 cal/g°C, the heat of transformation will cause a temperature rise of about 41°C. The actual temperature rise due to exothermic reaction in those high speed tests would be

$$41 \times .40 = 16.4°C$$

because only about 40% of austensite transformed.

strain. This is shown in Fig. 7. The highest temperature was reached as the specimens failed.

It should be pointed out, however, that temperature rise was very sudden and followed by a certain stationary period. This could be explained considering that the residual stresses were locked in the vicinity of the thermocouple after welding, thus causing the transformation to initiate at the thermocouple junction.

The locked-in stresses would have been reduced to a flow stress after some plastic deformation. Thus the situation will be such that the material around the welded spots are about to yield even before applying a load to the specimen.

The fact that the Lüders band very often started around the thermocouple could be regarded as evidence for this point. Thus the slope of the temperature rise curve for the material away from the thermocouple should be less steep than the recorded one. Therefore, it is not too surprising that the transformation was not completely suppressed in spite of the fact that the recorded temperature almost exceeded the M_D temperature at the end of testing.

The possible temperature rise under the adiabatic condition was calculated from the area under the true stress-strain curve using a numerical factor of 0.9[7] for the conversion of plastic work to heat evolution and it was seen that the calculated values reasonably agreed with the measured ones listed in Table III(b), signifying virtual establishment of the adiabatic situation. However, for the tests at 20 in/min, the calculated values were slightly lower than the measured values. The unusually high temperature rise measured very near the

fracture section was obviously due to the greater deformation at the neck.

Since the distance of the thermocouple from the fracture varied, the temperature rise just at the fracture was determined by extrapolation as about 250°C (Fig. 8). The calculations from true stress-strain curve based upon fracture area measurements showed values ranging from 250°C to 300°C.

This extrapolated value will be a temperature rise at the propagating crack front that experiences plastic deformation at a very high strain rate. Since heat transfer to the surroundings is negligible under the adiabatic condition, the martensite transformation of the material ahead of the crack tip will be greatly affected by the temperature rise only when the element under consideration approaches the M_D temperature as the crack proceeds.

Since plastic deformation, strain-induced martensite transformation, and heat evolution all can be considered to occur simultaneously, most of the martensite would form before the strain increased to the point where the M_D temperature was reached.

The liquid nitrogen test results in Table III (a) and (b) show that the temperature rise due to a high strain rate did not affect the martensite formation despite the lower specific heat at very low temperatures. At -196°C the specific heat (Cp) of the alloy is only about one-third of that at room temperature. Meanwhile the thermal conductivity (k) decreases to approximately half of the room temperature value. Therefore the thermal diffusivity ($\alpha = \frac{k}{\rho c}$, ρbeing the density of the material) at liquid nitrogen temperature will be 1.5 times as

great as at room temperature, although the decrease in specific heat value leads to an increased temperature rise. The use of water and liquid nitrogen baths instead of air for cooling would change the heat-flow conditions. The liquid bath would provide a better sink for the heat generated. Thus a strongly adiabatic condition would not prevail.

C. Variables Affecting Fracture Toughness

Fracture toughness can be assessed by the ratio of fracture energy to the area of rapid fracture (W/A). Previous work demonstrated that high-strength sheet materials in thickness down to about 0.040 inches can be satisfactorily tested by Charpy impact and slow bend using an edge-notch specimen similar to the standard V-notch Charpy specimen except for thickness. It was reported that the energy absorbed in the fracture of high-strength steels at high strain rates increased with increasing strain rate at a given temperature.[8] Photoelastic study has shown that a low strain-hardening material will exhibit a larger plastic enclave and hence improved crack resistance.[9] Therefore, the increased energy absorption at high strain rates could be explained in terms of increased plastic zone size if the strain hardening exponent decreases with increasing strain rate. A larger plastic zone size will allow increased energy absorption.

Since the sheets were so thin, it was believed that plane stress conditions prevailed during fracture.

Visual examination indicated that the material highly deformed during rolling fractured in a brittle manner while the specimen of lower prior deformation showed a ductile fracture. W/A values are given in Tables V and VI. It should be pointed out that not all of the

Charpy impact energy is spent by the plastic energy dissipation but about 30%[10] goes into producing shock waves in specimen and machine and accelerating the broken specimen halves to approximately the Charpy pendulum speed. Thus neglecting the contribution of surface tension required to create a new surface, only 70% will be dissipated plastically during the crack propagation.

In all cases the toughness decreased with an increasing amount of prior deformation and the trend was more pronounced for transverse specimens (Fig. 9). This anisotropic behavior suggests that with the transverse specimens the rolling direction, along which the precipitation of carbides during the rolling process might have been preferred, provides a perforation line for the propagating crack. Crack growth will be facilitated along the precipitate interface. Therefore, the smaller the amount of carbide precipitates, the higher will be the toughness. This can be illustrated by the specimens of 20% prior deformation showing superior toughness for the lower carbon content and for the lower rolling temperature at the same yield strength level (Table VIII).

The highest toughness for 20% prior deformation can be attributed to the lowest yield strength.* With the same amount of prior deformation,

---

* Half plastic zone size (1/2 R_p or r_p) can be calculated from the equation

$$r_p = 1/2\pi \left(\frac{K}{\sigma_{ys}} \right)^2 \qquad (10)$$

Thus the lower yield strength (σ_{ys}) would permit greater plastic energy dissipation at the same stress intensity (K).

a higher yield strength seems to be responsible for the lower toughness at a given temperature.

Fig. 17 shows that for all test temperatures the toughness decreases with increasing yield strength within a band or equivalently with increasing amount of prior deformation. It is interesting, however, to compare the specimens with the same yield strength level. For example, 675-3/90(450) (= 675-3 alloy rolled 90% at 450°C), 675-4/60(250) and 675-4/60(450) all have about the same yield strength when tested at room temperature, but their toughnesses are different. It can be seen that the toughness increases as the tensile strength or strain hardening rate decreases (Table VIII).

It will be recalled that the strain hardening rate has an inverse relationship with the tendency toward non-uniform deformation (Lüders strain) and, as discussed earlier, low strain hardening values tend to extend the plastic zone lengthwise resulting in a greater zone size and shape factor. Therefore, at the same stress intensity, lower strain hardening rates will give rise to a greater energy absorption.[3]

Fig. 18 shows this effect; W/A decreases linearly with increasing strain hardening rate at the same yield strength level and increases with decreasing yield strength. (In this plot strain hardening rates at the lowest test speed were used.)

From the temperature spectrum of W/A, it is obvious that strain-induced martensite transformation plays a role during fracture, viz., the drop in W/A, for above room temperature tests was due to suppression of the transformation near the M_D temperature; the yield strength

remained approximately unchanged. W/A decreased with decreasing test temperatures below room temperature, and also with increasing test temperatures above room temperature. A peak was obtained at room temperature. (Figs. 10 and 12).

Comparing relative magnitudes of decrease in toughness between different heats indicates that the degree of martensite contribution increases with increasing amount of prior deformation (Figs. 10 and 12). It is seen that the density of martensite bundles decreased as the distance from the fracture increased (Fig. 22). This had been expected since the plastic strain distribution in the transverse direction can be approximated by

$$\varepsilon_{p_\perp} = \left(\frac{R_p}{2r} - 1\right) \frac{\sigma_{ys}}{E} \qquad (11)$$

for a circular zone,[5] where r is the transverse distance from the crack.

Fig. 23 clearly shows that the martensite comes out along the macroscopic maximum shear planes through the thickness. It can be noted that the extent of the martensite zone was decreased to almost nil at midthickness.

The plastic zone height was measured utilizing offsets in the surface (Fig. 21) and also from the polished, then etched surface (Fig.22). These two measurements showed an excellent agreement. Furthermore, microhardness measurements also confirmed the above agreement indicating that the strain-induced martensite terminated at the elastic-plastic boundary (Fig. 13). Estimation of the martensite volume fraction based on the hardness measurements for the transformed tensile specimens were not available because of the difficulty in assessing the amount of strain hardening for austensite. Nor could estimations be made by the

grid intercept point count method from micrographs because of inadequate resolution of the structure.

To see if a higher loading rate could have possibly reduced the martensite transformation in impact tests, slow bend tests were run with three point loading. Measurements of absorbed energy by integrating the area under the load-deflection curve were not made because of the unusual load deflection curves obtained. These curves are shown in Fig. 14. At the minimum point in these curves, the crack had progressed to within about 0.003 in. of the opposite face, which was the point where the load was being applied. The concentrated load interfered with crack growth when the crack approached the face where the load was being applied.

Referring to Fig. 22(a) and (b) it appears that the martensite transformation was not enhanced when the loading rate was reduced by a factor of 10^5. As discussed earlier, this may be due to the concurrence of plastic deformation, heat evolution and strain-induced martensite transformation, that would result in incomplete suppression. It should be recalled that an adiabatic condition was already achieved at such a low speed as 0.4 in/min. It was observed that stable crack growth occurred at the stress intensity level ranging from 66 to 88* ksi-in$^{1/2}$

---

* Although a stress intensity factor K cannot be assigned to the material showing no instability point, it was calculated from the maximum load, P (at which "rapid" stable crack growth started) using the equation[11]

$$K = \frac{6Pa^{1/2}}{W}\left[1.93 - 3.07\left(\frac{a}{W}\right) + 14.53\left(\frac{a}{W}\right)^2 - 25.11\left(\frac{a}{W}\right)^3 + 25.80\left(\frac{a}{W}\right)^4\right] \quad (12)$$

where "a" is the depth of notch plus length of precrack and "W" the specimen width.

(Table VII). In the specimens of lower prior deformation, the crack growth proceeded at the rate of about 0.01 in/sec. all the way across the specimen width while, for higher prior deformation, the slow crack growth was followed by the fast fracture (Fig. 14). However, in impact tests, the absence of crack instability will be less likely to occur because of the high loading rate. For impact tests, K values were evaluated by the approximation

$$K_c \simeq (G_c E)^{1/2} \tag{13}$$

assuming 1:1 correlation between G_c and W/A.

Table VII indicates that these K values are greater than those obtained for slow bend tests and hence the plastic zone will be larger in impact tests. It is important that slow bend tests showed consistently smaller measurements of plastic height. Half plastic zone size, r_p, was calculated from Eq. 10. It was shown in Table VII that reasonable agreement was obtained between calculated and measured values for slow bend tests. A much greater discrepancy for impact tests may be partially due to the plastic enclave being extended lengthwise. Also improper substitution of the yield strength obtained at the lowest crosshead speed could be misleading in calculating the zone size for impact tests. The comparison between calculated zone "size" and measured zone "height" is shown in Fig. 15.

Since the lowest prior deformation corresponds to the greatest zone size, Fig. 16, where the energy absorption is plotted against the plastic zone height, illustrates that a greater slope for a greater zone height may be due to lower strain hardening values and increased stress intensity under impact conditions.

Fig. 20 (b) emphasizes that maximum toughness is obtained for the lowest prior deformation characterized by the lowest yield strength at the expense of tensile strength.

The data points at a given test temperature seem to fall on a single straight line having the same slope for various test temperatures on a semi-log plot of W/A vs tensile strength [Fig. 20(a)]. The straight line is represented by

$$\frac{W}{A} = ce^{-n\sigma_{TS}} \tag{14}$$

where "c" varies with the test temperatures.

In other words, the increase in tensile strength by the same difference will be accompanied by the decrease in W/A by the same ratio. At the same tensile strength level, for example, 260 ksi, it is seen that the specimen tested at -80°C shows a toughness $\frac{2000}{150} = 13.3$ times as high as the specimen tested at 200°C. This may be attributed to the strain-induced martensite transformation and the numerical factor of 13.3 could be predicted as follows: since the higher toughness above corresponds to 20% prior deformation, the transformation characteristics can be depicted by

$$V_{\alpha'} = 1.72\,\varepsilon^{1/2} \tag{15}$$

for dry ice test. However taking the triaxiality for the Charpy specimen into account,[12]

$$V_{\alpha'} = 1.72\,\varepsilon^{1/2} \times \frac{2}{1.2} = 2.87\,\varepsilon^{1/2}* \tag{16}$$

Then the separate contribution of the martensite, the austensite and the invariant shear to plastic energy dissipation (U) in front of the crack

---

* Strain rate effect was not taken into account.

will be expressed respectively by,[3]

$$U_{\alpha'} = 0.134\ \sigma_{\alpha'}\ (\frac{\sigma_c}{E})^{3/2}\ R_p{}^2 t \tag{17}$$

$$U_{\gamma} = 0.196\ \frac{\sigma_\gamma \sigma_c}{E}\ R_p{}^2 t - 0.134\ \sigma_c\ (\frac{\sigma_c}{E})^{3/2} R_p{}^2 t \tag{18}$$

$$U_{IS} = 0.442\ \sigma_{\alpha'}\ (\frac{\sigma_c}{E})^{1/2}\ \varepsilon_{IS} R_p{}^2 t \tag{19}$$

where the yield strength of the austenite, σ_γ, is approximated as the yield strength of the austenite-martensite mixture, σ_c = 150 ksi and the typical invariant shear strain, ε_{IS} = tan 19° = 0.344.

Since assuming the yield strength of the strain-induced martensite, $\sigma_{\alpha'}$, as about 350 ksi will not be too unreasonable, one obtains

$$U_{\alpha'} = 166\ R_p{}^2 t$$

$$U_{\gamma} = 76\ R_p{}^2 t$$

$$U_{IS} = 3760\ R_p{}^2 t$$

Therefore total contribution for one enclave (with a shape factor of $\frac{\pi}{8}$) will be

$$U_{\alpha'} + U_{\gamma} + U_{IS} = 4002\ R_p{}^2 t$$

In 200°C tests, there will be no strain-induced martensite transformation and the contribution will be due only to the austensite. Hence, the total will be

$$U_{\gamma} = 0.196\ \frac{\sigma_\gamma \sigma_c}{E}\ R_p{}'^2 t \tag{20}$$

For the specimen of 90% prior deformation pertains to the lower toughness,

$$\sigma_c \sim \sigma_\gamma = 217 \text{ ksi.}$$

Thus

$$U_{\gamma} = 309\ R_p{}'^2 t$$

Provided that the plastic zone size is the same, the ratio of plastic energy dissipation becomes

$$\frac{4002}{309} = 13.0$$

The plastic zone size, however, cannot be the same because of high yield strength for the specimen given a prior deformation of 90% that results in a smaller zone size. The lack of strain hardening at 200°C will give rise to a very narrow enclave having a shape factor of say, $\frac{\pi}{2}$ or greater. As a consequence, one might say at least qualitatively that these opposing factors in calculating the ratio of overall energy absorption tend to cancel each other leaving the value predicted above not drastically changed.

IV. SUMMARY AND CONCLUSIONS

1. The lower the yield strength, the higher is the toughness measured by W/A. At the same yield strength, lower strain hardening gives rise to improved crack resistance. These were attributed to the increase in contributing volume for plastic energy dissipation.

2. For all test temperatures, W/A and tensile strength showed a linear inverse relationship on a semi-log plot.

3. Yield strength and stress intensity factor for Charpy specimens were increased with increasing test speed whereas drops in the amount of martensite, strain hardening values, and tensile strength were severe.

4. The amount of martensite was reduced at the crosshead speed of 0.4 in/min. and remained approximately unchanged at higher speeds. The slow bend and Charpy impact tests did not show a recognizable difference in the martensite density (except for consistently smaller plastic zone heights in slow bend tests). These could be attributed to the adiabatic effect that does, but not completely, suppress the strain-induced martensite transformation.

5. The maximum toughness was obtained at room temperature for all heats and the role of strain-induced martensite in determining the fracture toughness was demonstrated by the decrease in W/A as the test temperature was raised to exceed the M_D. The comparison of the relative decrease in W/A indicates that the degree of contribution due to the strain-induced martensite increases with increasing amount of prior deformation.

6. The anisotropic effect of the specimens suggested that the role of carbide morphology could be significant.

Acknowledgments

The author wishes to thank Dr. V. F. Zackay, Prof. E. R. Parker and Mr. W. W. Gerberich for their research guidance, encouragements and support throughout the course of this investigation.

This work was performed under the auspices of the United States Atomic Commission through the Inorganic Research Division of the Lawrence Radiation Laboratory, Berkeley, California.

REFERENCES

1. L. Raymond, W.W. Gerberich and W.G. Reuter, On the Microstructural Sensitivity of Fracture Toughness, Aerospace Report TR-669 (6250-10)-7.

2. Y. Katz and M.D. Merz, Notch Toughness Variation in Steels with the Same Tensile Properties, Univ. of Calif., Berkeley; UCRL-18015, Dec. 1967.

3. W.W. Gerberich, P.L. Hemmings, V.F. Zackay and E.R.Parker, Interaction Between Crack Growth and Strain-Induced Transformation, Univ. of Calif., Berkeley; UCRL-18467, Sept. 1968.

4. B. De Miramon, M.S. Thesis, Univ. of Calif., Berkeley; UCRL-17849, Sept. 1967.

5. W.W. Gerberich, P.L. Hemmings and V.F. Zackay, Observations of Strain-Induced Martensite around a Crack, Univ. of Calif., Berkeley, UCRL-18534, Oct. 1968.

6. J.P. Bressanelli and A. Moskowitz, Trans.ASM 59, 223 (1966).

7. G.I. Taylor and H.Quinney, Proc. Roy. Soc. 143, 307 (1934).

8. G.M. Orner and C.E. Hartbower, Welding Journal 40, 405s (1961).

9. W.W. Gerberich, Exp. Mech. 4, 335 (1964).

10. G.A. Cottell, Some Sources of Error in Quasi-Static and Impact Notch Bar Testing, British Engine Boiler and Electrical Insurance Co. Technical Report,(1952).

11. British Iron and Steel Institute, Fracture Toughness, London, 1968, p. 55.

12. W.W. Gerberich, Private communication (from unpublished data).

FIGURE CAPTIONS

Fig. 1 Dimensions of tensile specimen (1 in. gage length).

Fig. 2 Dimensions of Charpy impact and slow bend specimens.

Fig. 3 Conventional stress-strain curve and corresponding ferromagnetic volumes (675-4 alloy given a prior deformation of 80% at 450°C: tested at room temperature using the crosshead speed of 0.04 in/min.).

Fig. 4 Characteristics of strain-induced martensite transformation (675-4 alloys) when tested at

a. room temperature

b. dry ice

c. liquid nitrogen.

Fig. 5 Strain hardening rate vs Lüders strain.

Fig. 6 Schematic load-extension curves at different crosshead speeds (675-3 alloy given a prior deformation of 60% at 250°C: tested at room temperature).

a. 0.04 in/min.

b. 0.4 in/min.

c. 5 in/min.

d. 20 in/min.

Fig. 7 Change of specimen temperature with time (675-3 alloys tested at room temperature using the corsshead speed of 20 in/min.).

Fig. 8 Temperature change with distance from the fracture (same specimens as in Fig. 7).

Fig. 9 Fracture toughness (W/A) of 657-3 alloys varying with the amount of prior deformation at

a. 250°C

b. 450°C.

Fig. 10 Toughness-test temperature profile of 675-3 alloys given a prior deformation at

a. 250°C

b. 450°C.

Fig. 11 Toughness of 657-4 alloys varying with the amount of prior deformation at

a. 250°C

b. 450°C.

Fig. 12 Toughness-test temperature profile of 657-4 alloys given a prior deformation at

a. 250°C

b. 450°C.

Fig. 13 Microhardness measurements for a Charpy impact specimen(657-4 alloy given a prior deformation of 90% at 450°C: tested at room temperature).

Fig. 14. Load-deflection curves for slow bend test (675-4 alloys).

Fig. 15 Comparison of half plastic zone heights between Charpy impact and slow bend tests. (675-4 alloys tested at room temperature.)

Fig. 16 Toughness vs half plastic zone height for Charpy impact specimens (675-4 alloys tested at room temperature).

Fig. 17 Toughness vs yield strength (625-4 alloys).

Fig. 18 Fracture toughness as a function of strain hardening rate and lower yield point.

Fig. 19 Toughness vs tensile strength (675-3 alloys).

Fig. 20 Toughness vs tensile strength (675-4 alloys) with varying

a. test temperature

b. amount of prior deformation

Fig. 21 Comparison of plastic zones formed during tests at room temperature (675-4 alloys given a prior deformation of 60% at 450°C).

a. Slow bend test: $1/2\ H_p = 0.017$ in.

b. Charpy impact test: $1/2\ H_p = 0.024$ in.

Fig. 22 Micrographs of the surface around the fracture (same specimen as in Fig. 21(b): Charpy impact test), x63. Nickel plating on the fractured surface appears white.

Fig. 23 Micrographs of thickness section cut perpendicular to the direction of crack (same specimens as in Fig. 21), x63

a. Slow bend test

b. Charpy impact test

Table I. Tensile Properties of the Alloys

Test Temp. °C	Heat	675-3				675-4			
		%EL	YS $\times 10^3$psi	TS $\times 10^3$psi	$V_{\alpha'}$ %	% EL	YS $\times 10^3$psi	TS $\times 10^3$psi	$V_{\alpha'}$ %
22	20 (250)	37.8	123	201	77.1	57.4	138*	196	62.2
	60 "	31.9	178	229	76.9	42.6	205	222	55.2
	80 "	38.0	213	236	72.5	32.5	232	237	53.6
	90 "	39.4	235	262	75.0	35.5	243	249	57.8
	20 (450)	58.2	138	196	72.1	49.2	139	192	69.8
	60 "	31.9	176	230	80.5	34.3	202	250	75.2
	80 "	32.7	198	254	83.0	32.7	221	271	76.8
	90 "	30.3	201	264	82.0	33.8	224	283	78.2
-80	20 (250)	-				24.4	150	272	79.4
	60 "	-				23.0	219	317	78.6
	80 "	-				23.8	242	335	79.3
	90 "	-				22.5	263	342	79.3
	20(450)	-				24.4	149	285	82.9
	60 "	-				20.7	182	325	82.8
	80 "	-				22.1	208	345	85.6

Table I., continued

Test Temp. °C	Heat	675-3				675-4			
		% EL	YS $\times 10^3$psi	TS $\times 10^3$psi	$V_{\alpha'}$ %	%EL	YS $\times 10^3$psi	TS $\times 10^3$psi	$V_{\alpha'}$ %
	90 (450)	-				19.7	216	357	86.3
-196	20 (250)	16.2	144	299	79.7	8.0†	177	(172)	49.9
	60 "	-				16.7	233	372††	76.6
	80 "	-				17.7	262	360	78.0
	90 "	-				15.0	287	383	71.7
	20 (450)	18.9	132	291	77.4	13.4†	145	279	69.4
	60 "	-				10.5†	199	255	64.2
	80 "	-				10.9†	230	301	71.1
	90 "	20.5	202	369	64.3	12.2†	231	281	66.5
100	20 (250)	-				11.4	128*	134	1.4
	60 "	-				3.2	196*	206	1.8
	80 "	4.7	189*	203	4.3	3.9	229*	248	8.5
	90 "	-				5.9	242*	263	11.9
	20 (450)	-				18.9	131*	140	1.9

Table I., continued

Test Temp. °C	Heat	675-3				675-4			
		% EL	YS $\times 10^3$psi	TS $\times 10^3$psi	$V_{\alpha'}$ %	% EL	YS $\times 10^3$psi	TS $\times 10^3$psi	$V_{\alpha'}$ %
	60 (450)	-				3.5	194*	208	1.8
	80 "	45.2	195*	204	38.5	12.4	218*	238	10.9
	90 "	-				9.8	221*	247	14.7
200	20 (250)	-				7.3	126*	132	0.9
	60 "	-				5.7	189*	199	1.0
	80 "	5.5	187*	202	3.3	-			
	90 "	-				4.5	219*	238	5.6
	20 (450)	-				5.5	126*	129	1.2
	60 "	-				4.5	187*	200	1.3
	80 "	5.5	185*	193	1.6	-			
	90 "	-				4.7	214*	231	1.4

$V_{\alpha'}$ = volume fraction of martensite measured at the time of fracture

20 (250), etc. = 20% prior deformation at 250°C, etc.

* 0.2% yield offset

† premature failure

†† fracture at pinhole

Table II. Characteristics of Strain-Induced Martensite Transformation (m/p/m' according to $V_{\alpha'} = m\,\varepsilon^{p}$ or $V_{\alpha'} = m'\,\varepsilon^{1/2}$) for 675-4 alloy

Heat \ Test Temp °C	22	-80	-196
60 (250)			
80 "	$(m')_{avg} = 0.85$	1.75	1.90
90 "			
60 (450)			
80 "	$(m')_{avg} = 1.40$	1.90	1.95
90 "			
20 (250)	1.15/0.93/0.80	1.70/0.51/1.67	
60 "	1.05/0.70/0.84	1.60/0.46/1.70	1.90/0.51/1.90
80 "	0.95/0.56/0.89	1.50/0.42/1.75	
90 "	0.50/0.22/0.88	1.40/0.38/1.75	
20 (450)	1.35/0.88/0.95	1.70/0.45/1.81	
60 "	1.25/0.45/1.32	1.60/0.38/1.95	1.95/0.50/1.95
80 "	1.15/0.36/1.40	1.55/0.37/1.96	
90 "	1.10/0.30/1.43	1.50/0.34/2.00	

Table III (a). Strain Rate Effects on Tensile Properties for 657-3 Alloy.

Heat \ Crosshead Speed, in/min.	0.04	0.4	5	20
	22°C Test			
20 (250)	% EL = 37.8	-	-	26.4
	YS = 123/120*			-/142
	TS = 201			159
	$V_{\alpha'}$ = 77.1			24.3
60 "	% EL = 31.9	20.1	22.3	18.4
	YS = 178/168	181/166	-/168	-/180
	TS = 229	187	192	195
	$V_{\alpha'}$ = 76.9	42.1	43.5	45.1
80 "	% EL = 38.0	-	-	16.8
	YS = 213/197			-/204
	TS = 236			211
	$V_{\alpha'}$ = 72.5			38.3
90 "	% EL = 39.4	15.4	7.2	7.0
	YS = 235/221	240/221	-/229	-/226
	TS = 262	(223)**	(231)	252
	$V_{\alpha'}$ = 75.0	38.9	28.5	30.5

Table III (a).,continued

Heat \ Crosshead Speed in/min.	0.04	0.4	5	20
20 (450)	% EL = 58.2	-	36.1	31.2
	YS = 138/136		-/134	-/134
	TS = 196		157	167
	$V_{\alpha'}$ = 72.1		28.5	37.5
60 "	% EL = 31.9	-	22.1	22.8
	YS = 176/162		-/174	-/177
	TS = 230		196	200
	$V_{\alpha'}$ = 80.5		51.6	49.5
80 "	% EL = 32.7	-	-	23.2
	YS = 198/183			-/194
	TS = 254			210
	$V_{\alpha'}$ = 83.0			53.5
90 "	% EL = 30.3	22.1	24.5	22.0
	YS = 201/196	215/204	-/213	-/206
	TS = 264	(206)	220	224
	$V_{\alpha'}$ = 82.0	48.3	46.0	55.8

Table III (a)., Continued

Heat \ Crosshead Speed, in/min.	0.04	0.4	5	20
	-196°C Test			
20 (250)	% EL = 16.2 YS = 144/130 TS = 299 $V_{\alpha'}$ = 79.7	-	-	15.6 -/143 267 80.9
20 (450)	% EL = 18.9 YS = 132/127 TS = 291 $V_{\alpha'}$ = 77.4	-	-	19.6 -/129 266 84.0

YS and TS, $\times 10^3$ psi; $V_{\alpha'}$, %

* $\sigma_{UYP}/\sigma_{LYP}$

** ( ) indicates that the specimen failed without showing the region of apparent strain hardening.

Table III (b). Measured Temperature Rise within Specimen above Test Temperature. °C

Heat \ Crosshead Speed in/min.	5	20
	22°C Test	
20 (250)	-	82 (0.18)*
60 "	75 (0.36)	129 (0.05)
80 "	-	88 (0.53)
90 "	-	141 (0.10)
20 (450)	84 (0.38)	93 (0.20)
60 "	109 (0.09)	103 (0.29)
80 "	-	170 (0.02)
90 "	88 (0.45)	103 (0.18)
	-196°C Test	
20 (250)	-	-
20 (450)	-	86 (0.46)

* ( ) indicates the distance of thermocouple from the fracture (in.)

Table IV (a). Strain Hardening Characteristics (A, × 10^3 psi/n according to $\sigma_T = A\,\varepsilon_T^{\,n}$) for 675-3 Alloy at Room Temperature

Heat \ Test Speed in/min.	0.04	0.4	5	20
20 (250)	535/0.57	-	-	300/0.29
60 "	515/0.41	300/0.18	395/0.33	380/0.29
80 "	460/0.35	-	-	435/0.29
90 "	530/0.38	-	-	-
20 (450)	445/0.56	-	310/0.35	360/0.36
60 "	540/0.45	-	510/0.49	440/0.37
80 "	710/0.58	-	-	465/0.38
90 "	680/0.51	640/0.57	620/0.54	460/0.33

Table IV (b). Lüders Strain (ε_L, %) for the Same Alloy at Room Temperature.

Heat \ Test Speed in/min.	0.04	0.4	5	20
20 (250)	9.5	-	-	7.5
60 "	7.9	5.9	11.2	11.8
80 "	10.6	-	-	16.9
90 "	15.4	-	-	-
20 (450)	14.2	-	13.8	13.1
60 "	11.4	-	13.4	13.5
80 "	12.2	-	-	15.2
90 "	11.0	15.4	18.2	15.0

Table IV (c) True Fracture Stress & Strain (σ_f, $\times 10^3$psi/ ε_f, %) for the Same Alloy

Heat \ Test Speed in/min.	22°C Test		-196°C Test	
	0.04	20	0.04	20
20 (250)	315/63	308/65	-	463/56
60 "	353/70	358/61	-	-
80 "	391/59	378/58	-	-
90 "	413/54	381/56	-	-
20 (450)	348/75	321/68	-	458/58
60 "	351/60	346/57	-	-
80 "	397/61	364/53	-	-
90 "	431/63	404/61	-	-

Table V Fracture Toughness (W/A, in-lb/in^2) of 675-3 Alloy

Heat \ Test Temp. °C	-196	22	22 (longitudinal specimen)	200
20 (250)	823	2970	3040	2410
60 "	503	1690	2310	925
80 "	362	994	2010	464
90 "	262	581	1565	231
20 (450)	964	2880	3010	2680
60 "	469	1620	2750	867
80 "	380	1025	2290	519
90 "	364	725	2180	310

Table VI Fracture Toughness (W/A, in-lb/in^2) of 675-4 Alloy

Heat \ Test Temp. °C	-196	-80	-30	22	100	200
20 (250)	392	1630	2060	2460	2320	1880
60 "	235	622	902	1062	875	572
80 "	218	472	535	649	370	265
90 "	184	420	413	456	285	186
20 (450)	363	1270	1700	2360	2340	2250
60 "	205	563	635	963	996	771
80 "	178	294	369	475	424	253
90 "	136	275	287	422	415	243

Table VII Plastic Zone Sizes for 675-4 Alloy
Tested At Room Temperature

	Slow Bend Test				Charpy Impact Test			
Heat	K KSi - $in^{1/2}$	K/σ_{YS} $in^{1/2}$	(R_P) calc in	$(1/2\ H_P)$ obs in	K KSi - $in^{1/2}$	K/σ_{YS} $in^{1/2}$	(R_P) calc in	$(1/2\ H_P)$ obs in
20 (250)	68.5	0.496	0.039	0.028	272	1.970	0.619	0.040
60	87.6	0.428	0.029	0.019	179	0.873	0.121	0.026
80	79.9	0.344	0.019	0.014	140	0.603	0.058	0.014
90	76.2	0.313	0.016	0.010	117	0.481	0.037	0.013
20 (450)	66.0	0.475	0.036	0.028	266	1.915	0.583	0.038
60	75.0	0.371	0.022	0.017	170	0.841	0.113	0.024
80	71.0	0.321	0.016	0.011	119	0.538	0.046	0.013
90	69.2	0.309	0.015	0.009	113	0.504	0.040	0.013

-43-

Table VIII (a) Correlation Between Tensile and Impact Properties for 675-3 Alloy

Test Temp. °C	Heat	σ_{LYP} X10^3 psi	ϵ_L %	$(V_{\alpha'})_{\epsilon_L}$ * %	$\partial\sigma_T/\partial\epsilon_T$ X10^3 psi	W/A in-lb/in^2
22	20 (250)	120	9.5	--	742	2970
	60 "	168	7.9	--	710	1690
	80 "	197	10.6	--	623	994
	90 "	221	15.4	--	644	581
	20 (450)	136	14.2	--	462	2880
	60 "	162	11.4	--	793	1620
	80 "	183	12.2	--	955	1025
	90 "	196	11.0	--	1025	725
-196	20 (250)	130	5.9	--	2540	823
	60 "	--	--	--	--	--
	80 "	--	--	--	--	--
	90 "	--	--	--	--	--
	20 (450)	127	6.3	--	1880	964
	60 "	--	--	--	--	--
	80 "	--	--	--	--	--
	90 "	194	8.7	--	2910	364

Table VIII (b) 675-4 Alloy

Test Temp. °C	Heat	σ_{LYP} X10^3 psi	ϵ_L %	$(V_{\alpha'})\epsilon_L$ * %	$\partial\sigma_T/\partial\epsilon_T$ X10^3 psi	W/A in-lb/in^2
22	20 (250)	142	13.4	14	398	2460
	60 "	193	16.2	29	433	1062
	80 "	218	20.9	40	484	649
	90 "	225	18.1	42	537	456
	20 (450)	133	11.6	20	515	2360
	60 "	188	12.8	45	824	963
	80 "	205	11.8	53	908	475
	90 "	215	11.6	54	1035	422
-80	20 (250)	131	9.5	--	1555	1630
	60 "	193	9.5	--	1865	622
	80 "	224	10.2	--	2060	472
	90 "	250	10.6	--	2310	420
	20 (450)	127	6.7	--	1835	1270
	60 "	174	7.9	--	2455	563
	80 "	195	7.7	--	2520	294
	90 "	204	8.3	--	2570	275

Table VIII (b) Continued

Test Temp. °C	Heat	σ_{LYP} X10^3 psi	ϵ_L %	$(V_{\alpha'})_{\epsilon_L}$* %	$\partial\sigma_T/\partial\epsilon_T$ X10^3 psi	W/A in-lb/in^2
-196	20 (250)	155	7.3	40	2940	392
	60 "	219	8.3	46	2730	235
	80 "	248	9.9	49	2595	218
	90 "	272	9.3	50	2600	184
	20 (450)	137	5.7	36	2335	363
	60 "	188	7.1	49	3200	205
	80 "	216	7.3	51	3070	178
	90 "	221	8.7	50	2950	136

* Martensite volume fraction measured at Lüders strain.

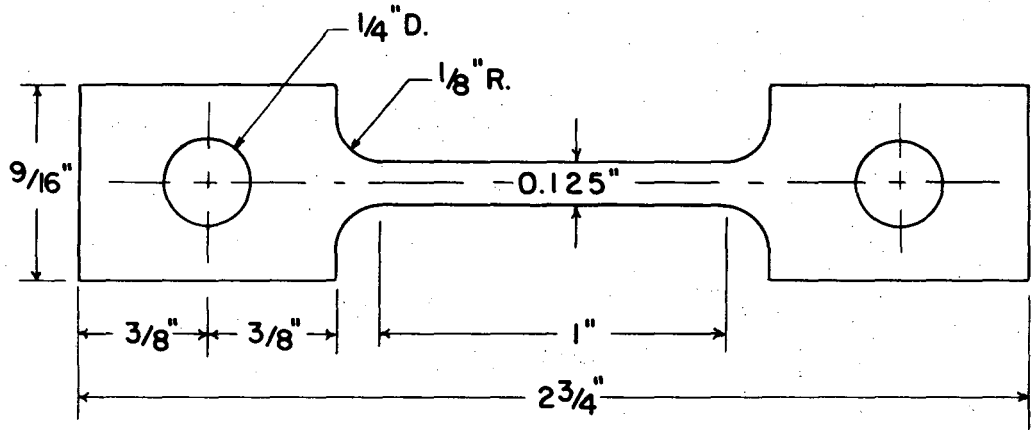

Fig. 1

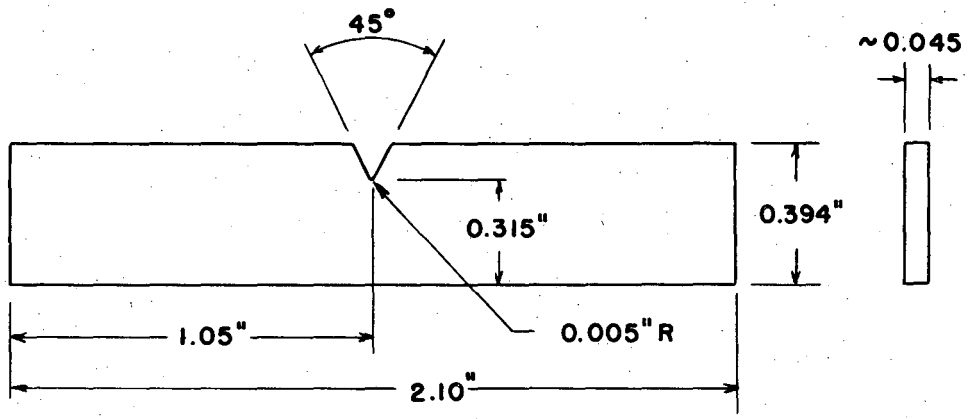

XBL 698-1282

Fig. 2

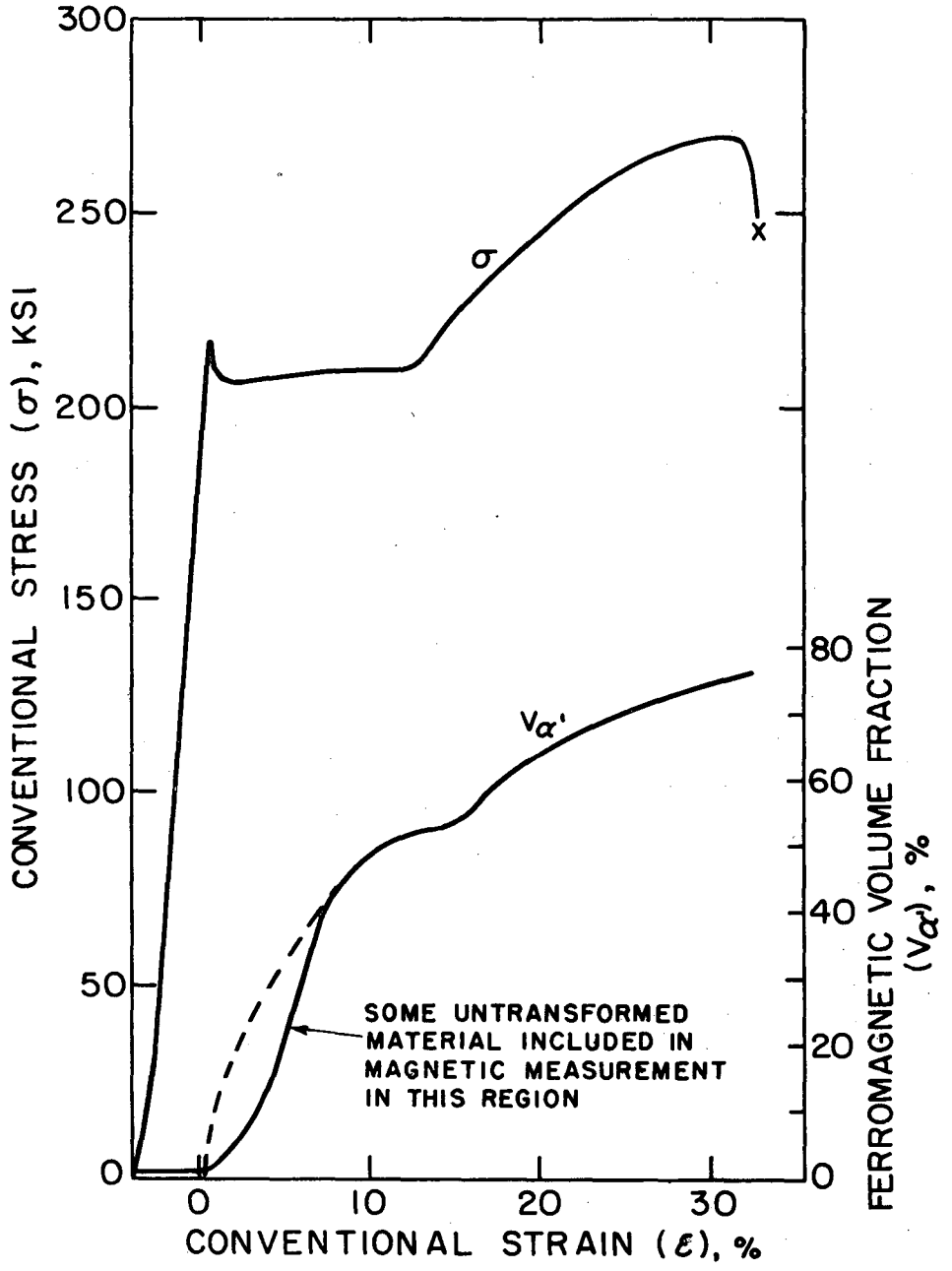

XBL 698-1283

Fig. 3

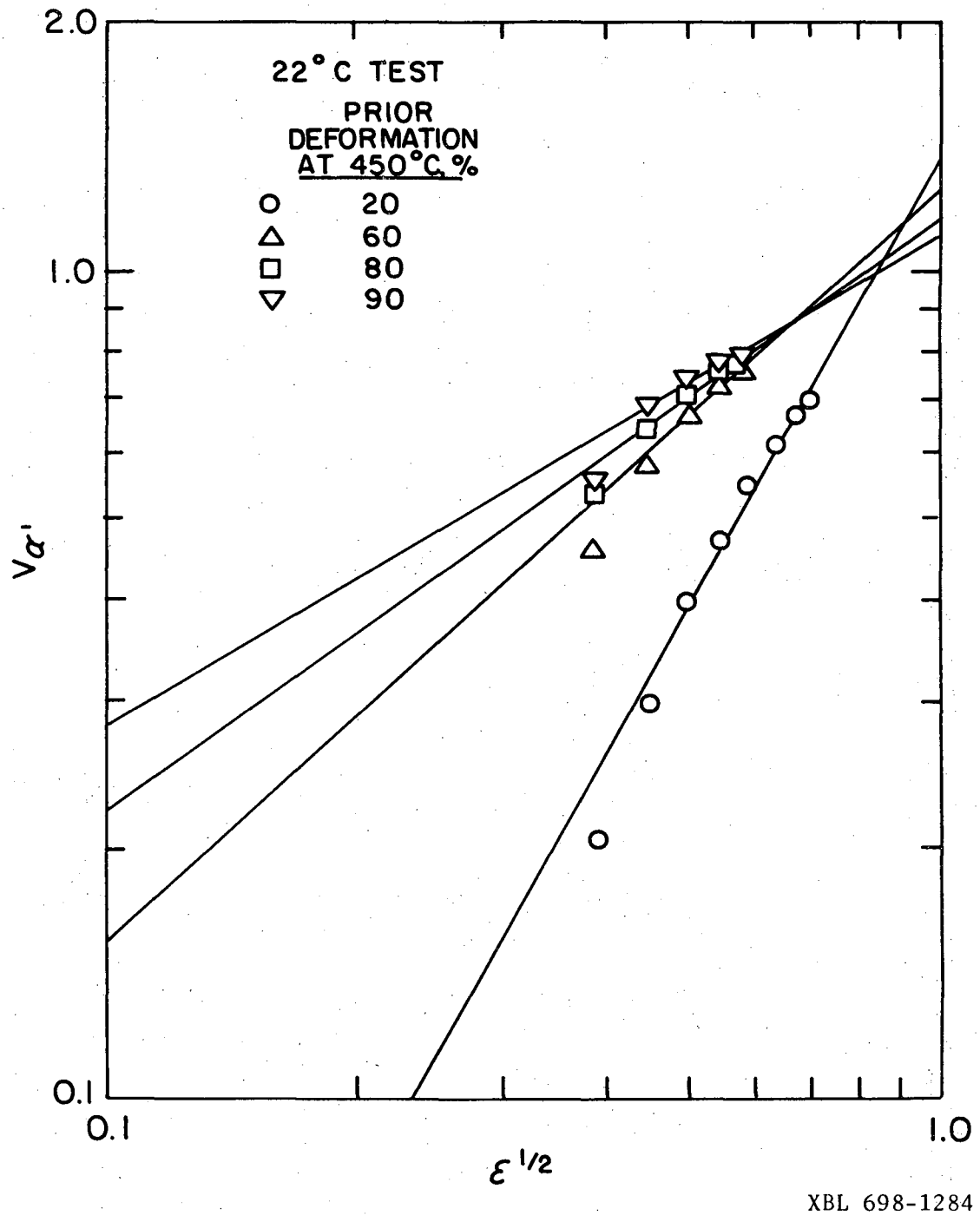
2.0
1.0
0.1
0.1
1.0
22° C TEST
PRIOR
DEFORMATION
AT 450°C, %
20
60
80
90
Vα'
ε 1/2
XBL 698-1284

Fig. 4(a)

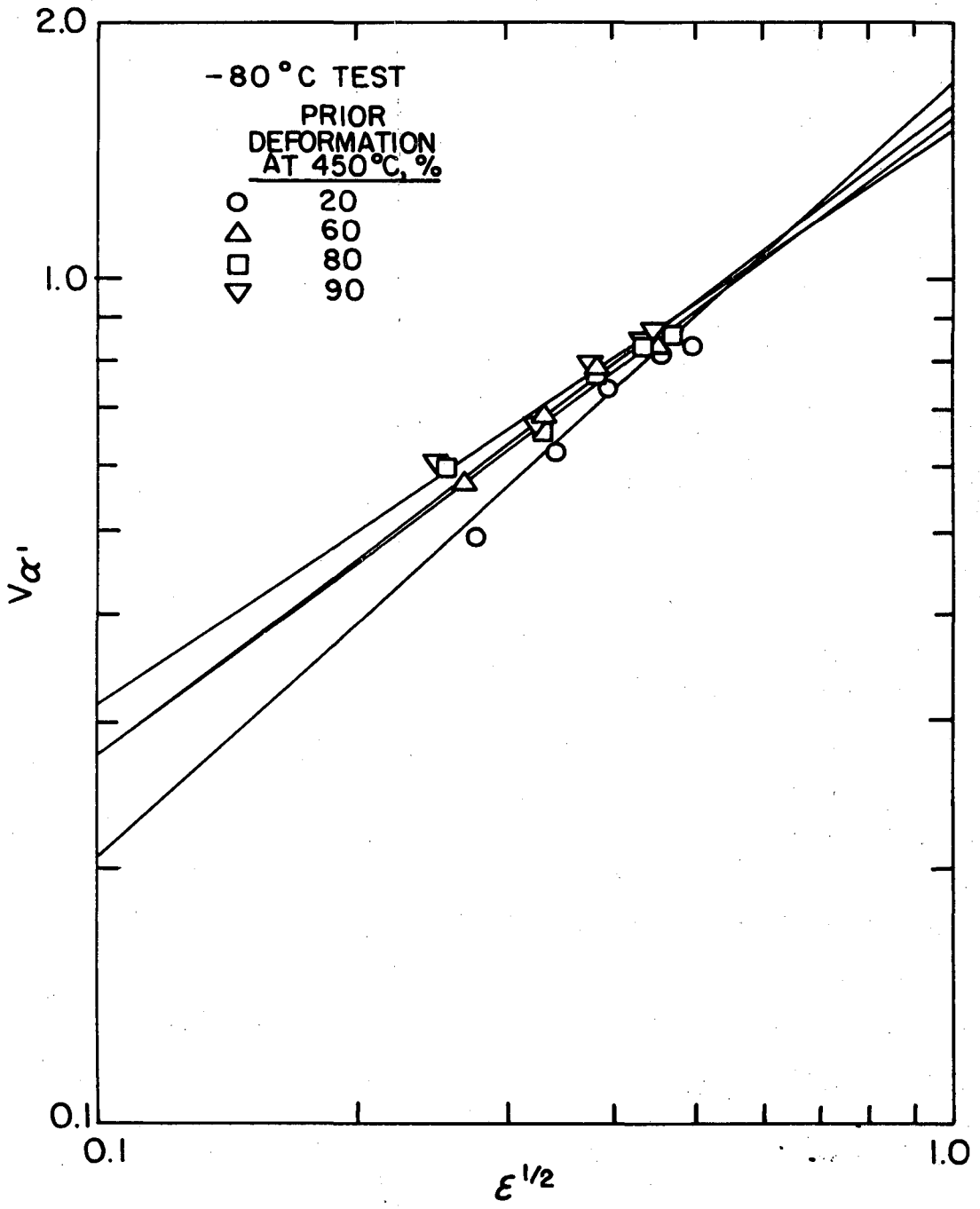

XBL 698-1285

Fig. 4(b)

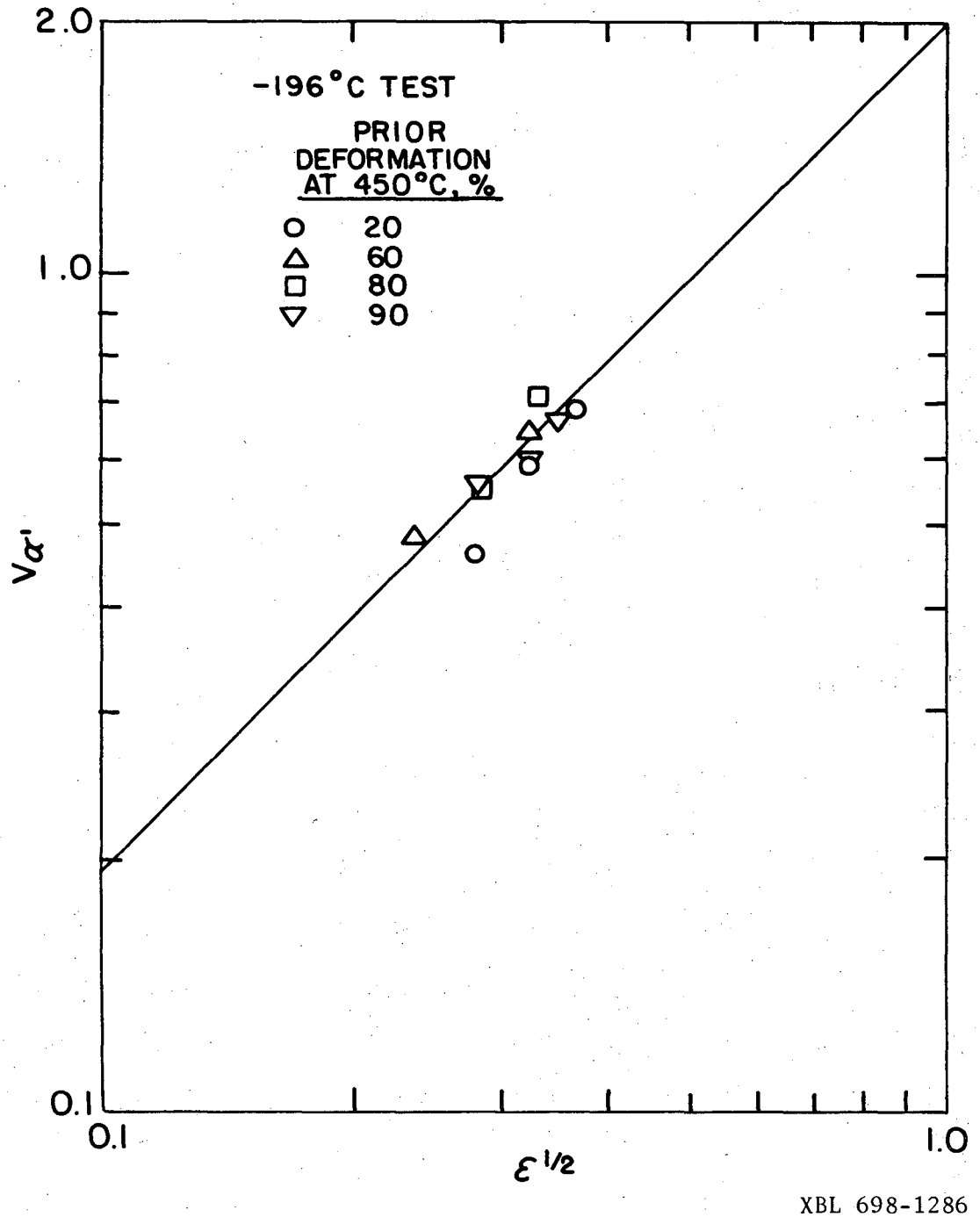

XBL 698-1286

Fig. 4(c)

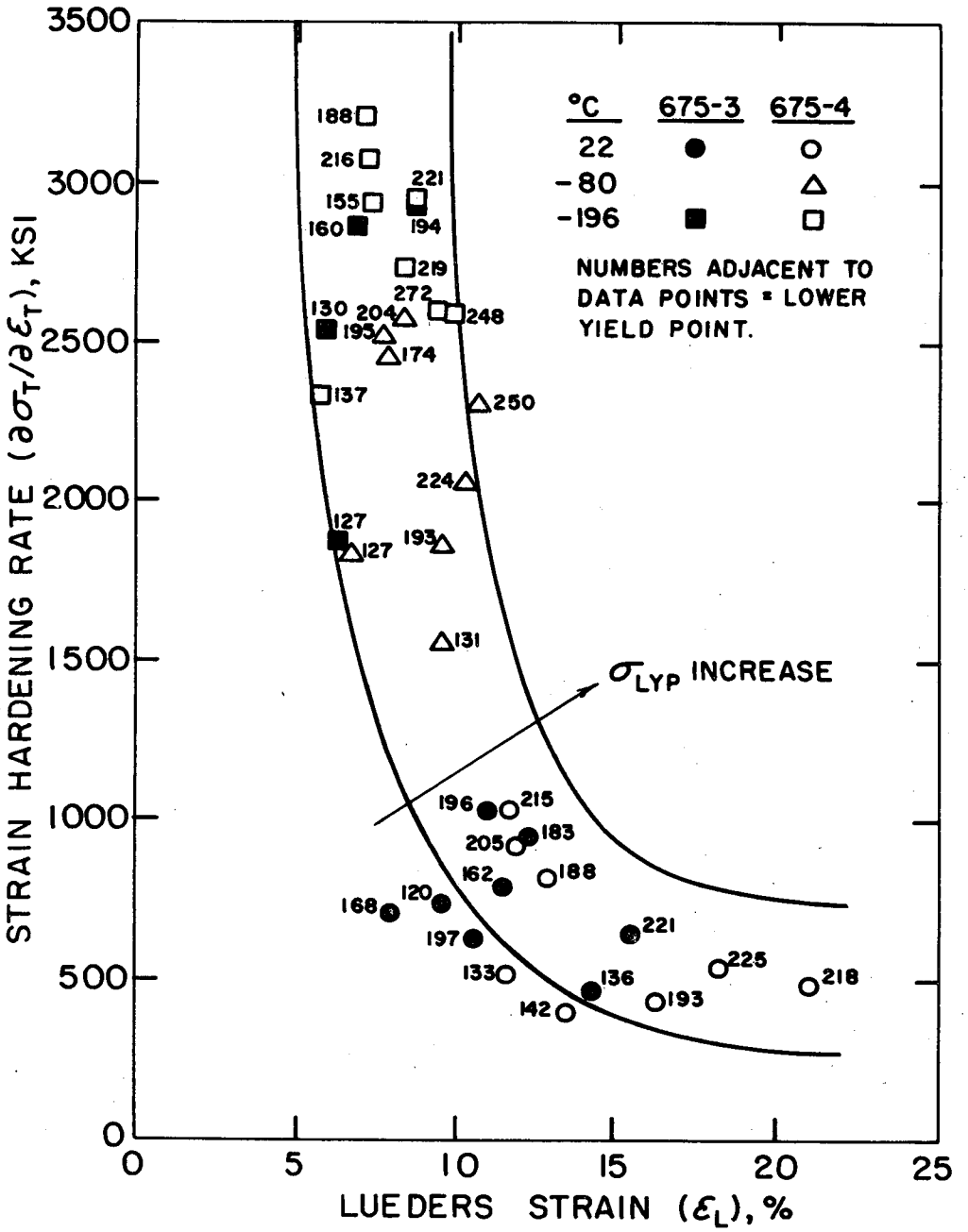

XBL 698-1287

Fig. 5

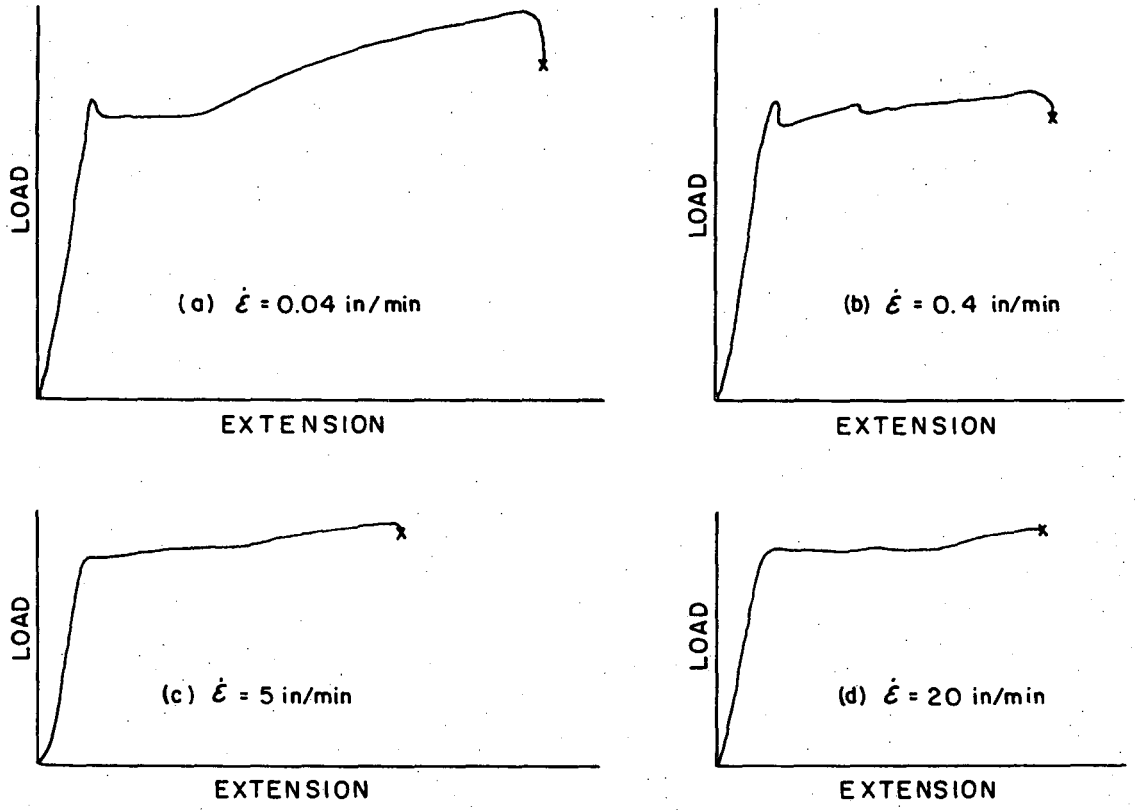

XBL 698-1288

Fig. 6

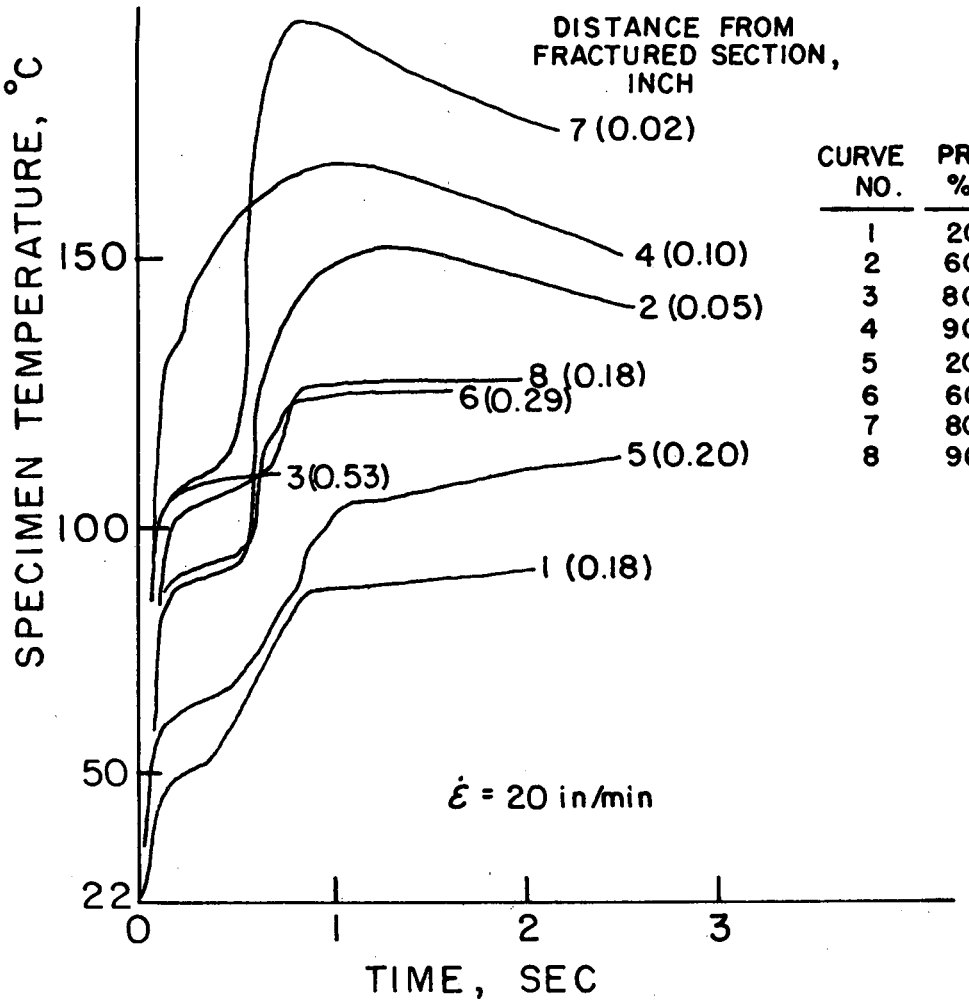

XBL 698-1289

Fig. 7

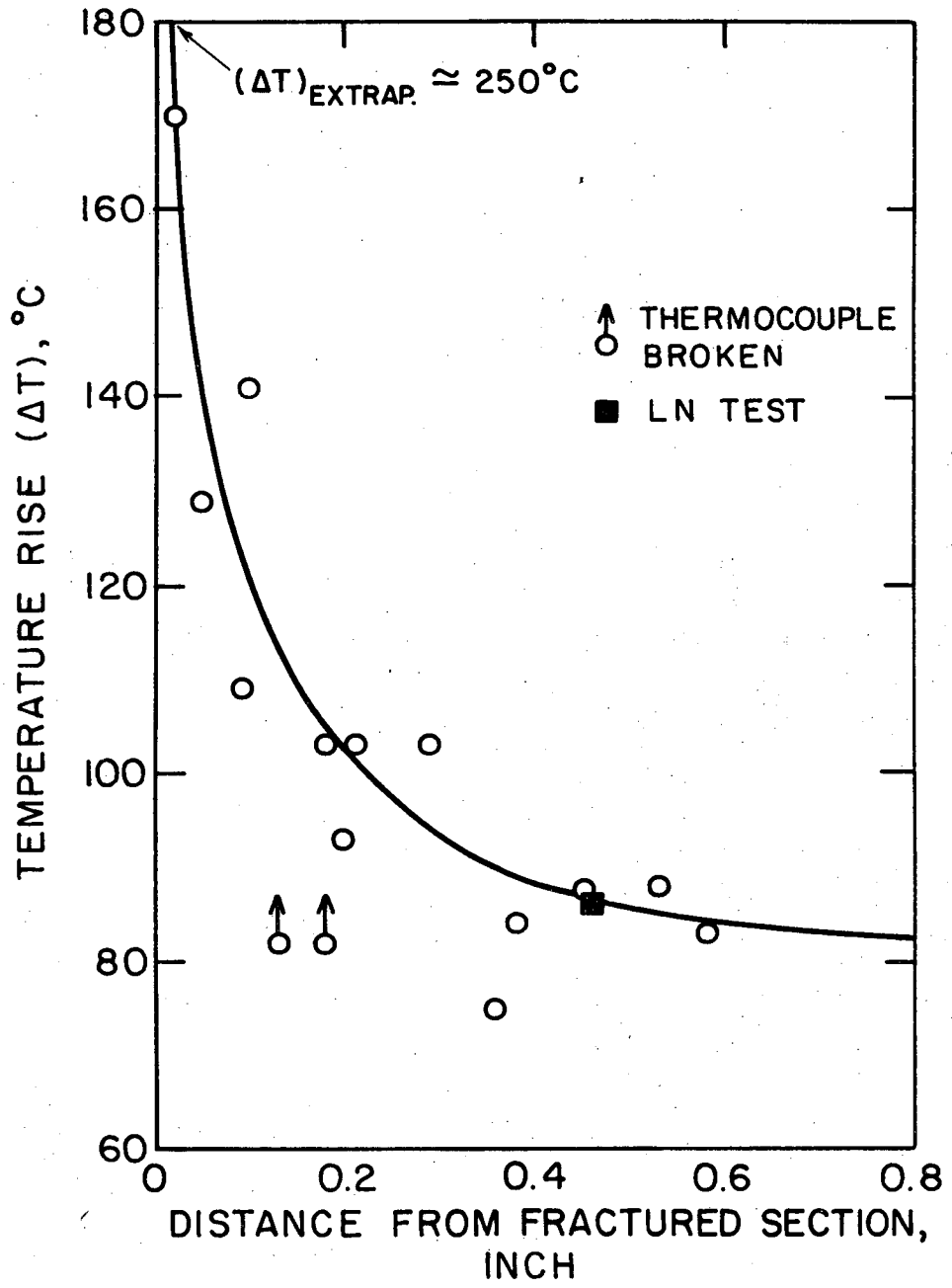

XBL 698-1290

Fig. 8

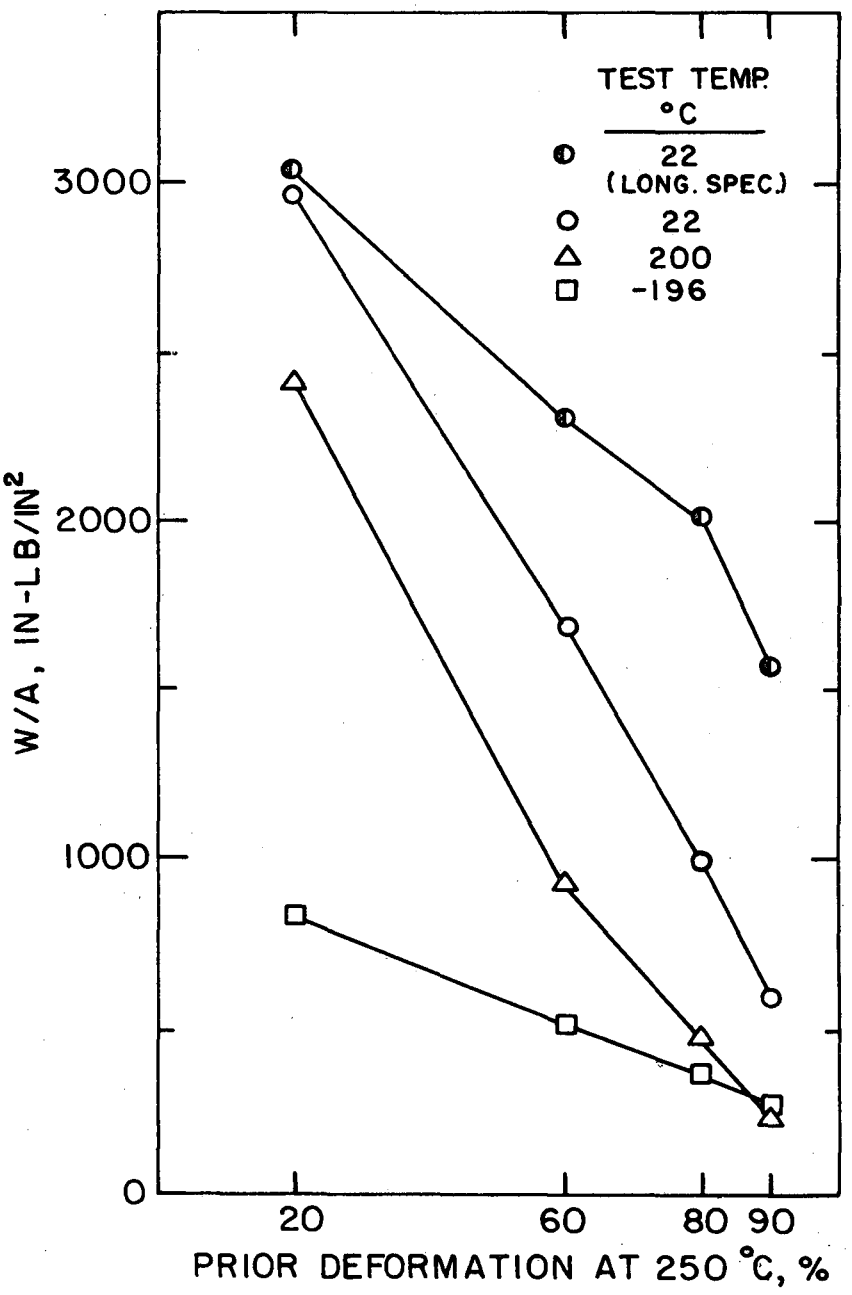

XBL 698-1291

Fig. 9(a)

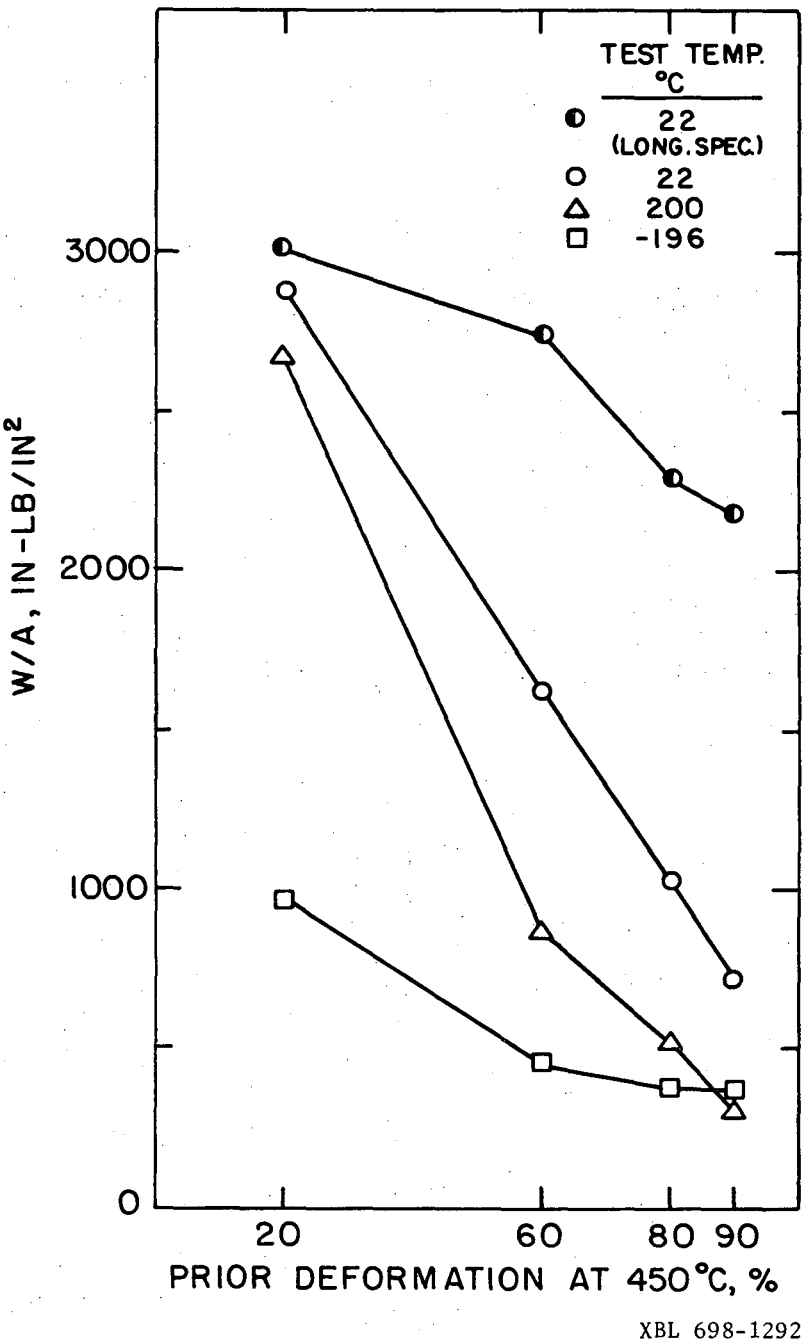
TEST TEMP. °C
22 (LONG. SPEC.)
22
200
-196
3000
2000
1000
0
W/A, IN-LB/IN²
20
60
80 90
PRIOR DEFORMATION AT 450°C, %
XBL 698-1292

Fig. 9(b)

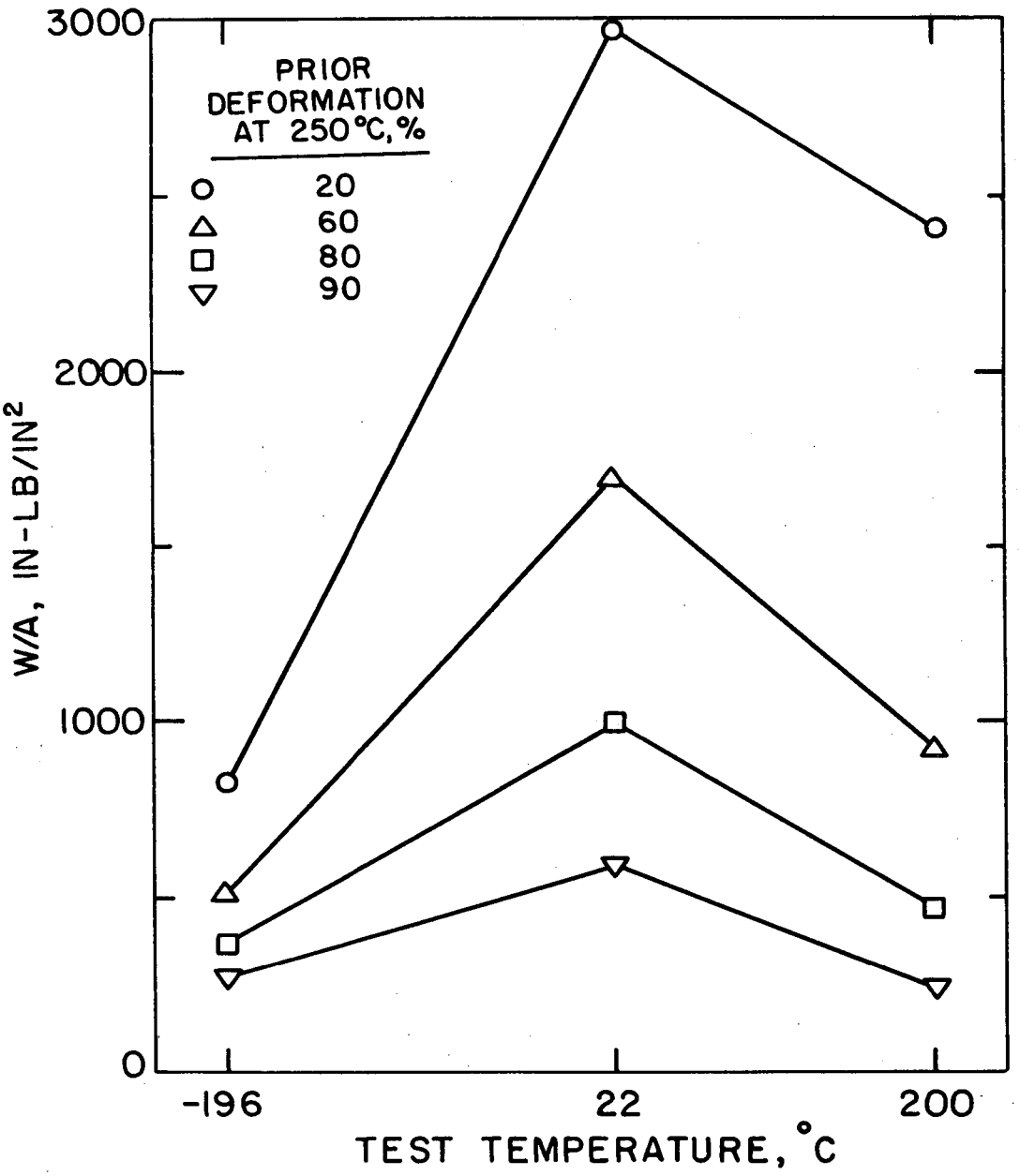
3000
2000
1000
0
W/A, IN-LB/IN²
PRIOR
DEFORMATION
AT 250°C, %
20
60
80
90
-196
22
200
TEST TEMPERATURE, °C
XBL 698-1293

Fig. 10(a)

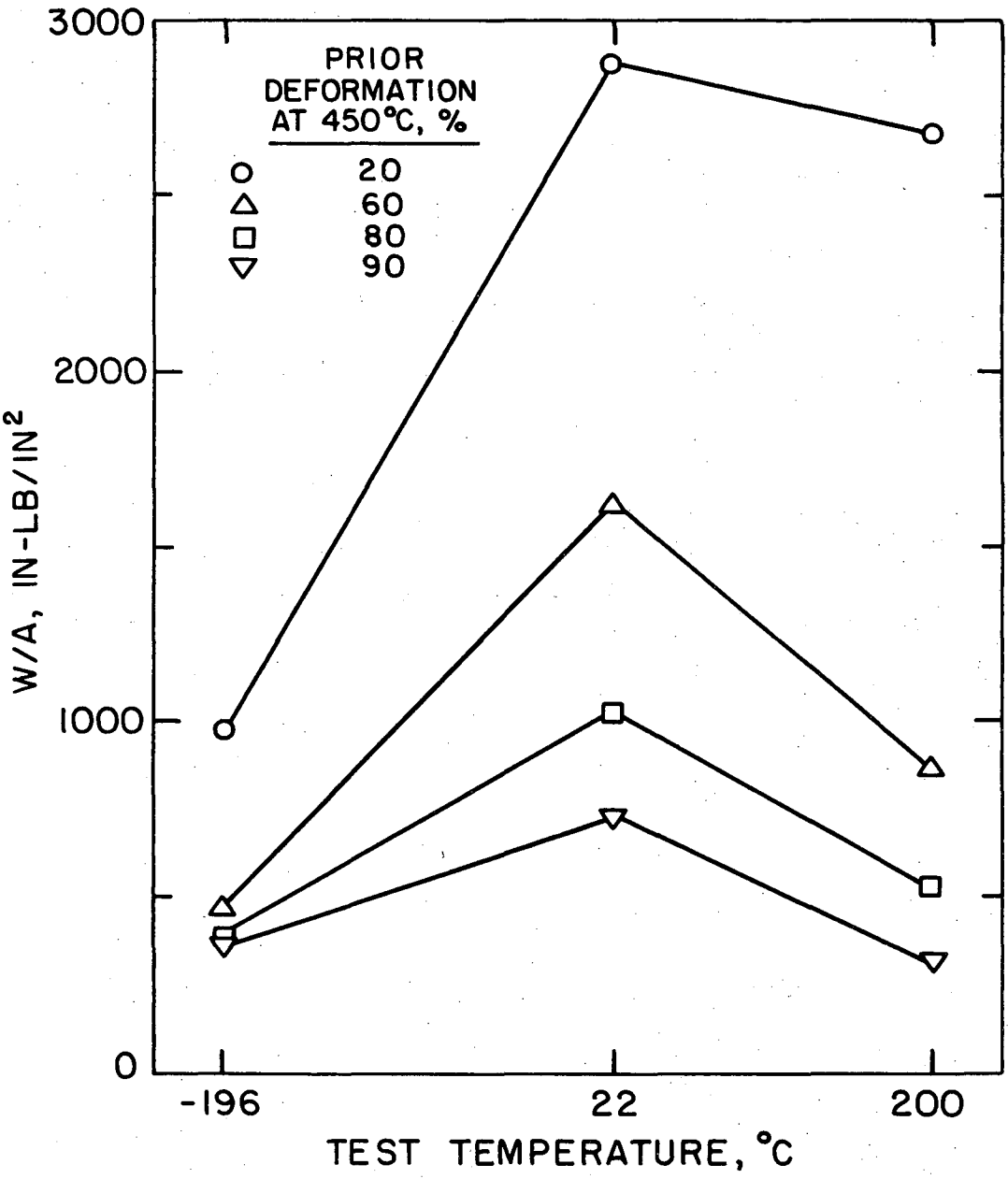

XBL 698-1294

Fig. 10(b)

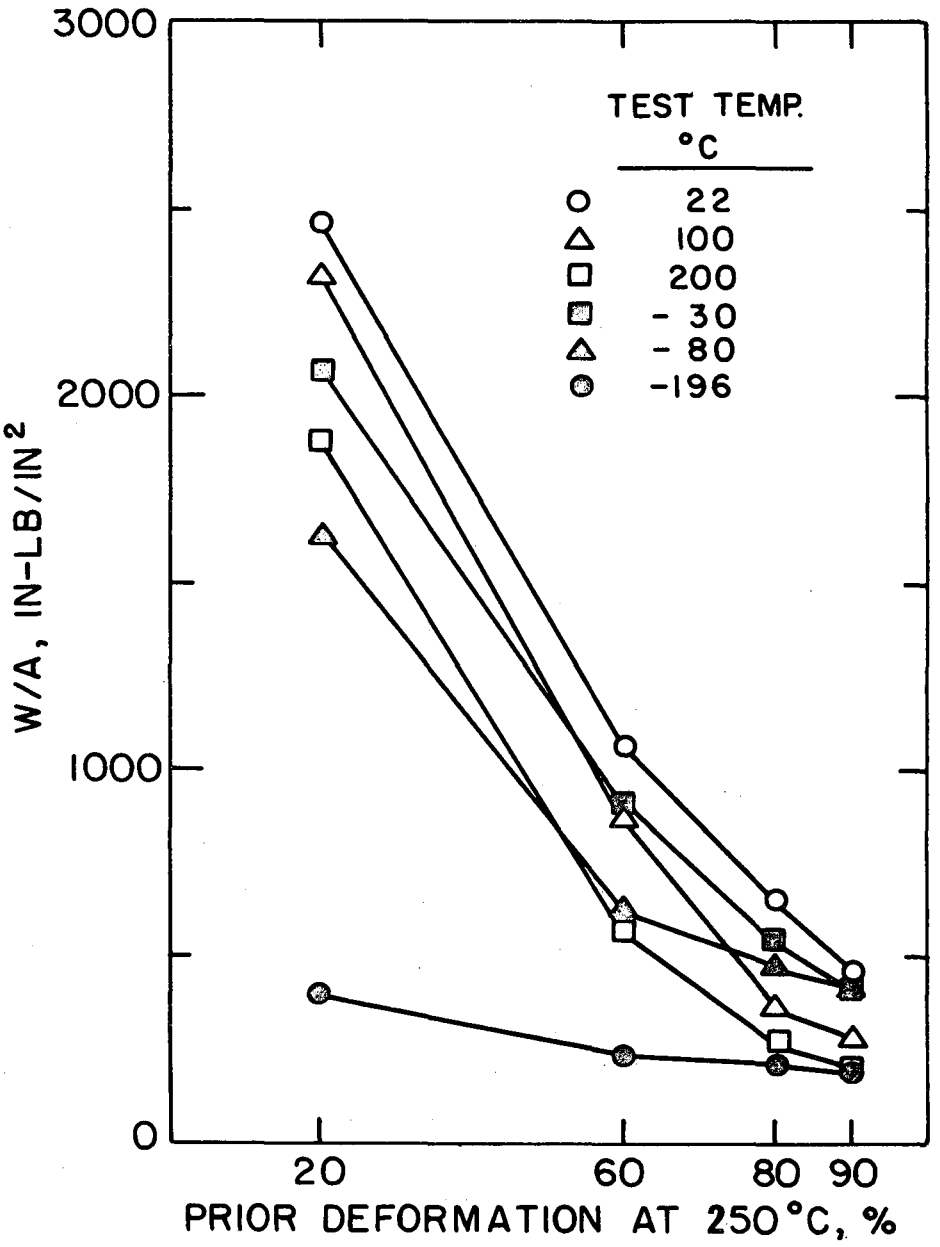
3000
2000
1000
0
W/A, IN-LB/IN²
TEST TEMP. °C
22
100
200
- 30
- 80
-196
20
60
80
90
PRIOR DEFORMATION AT 250°C, %
XBL 698-1295

Fig. 11(a)

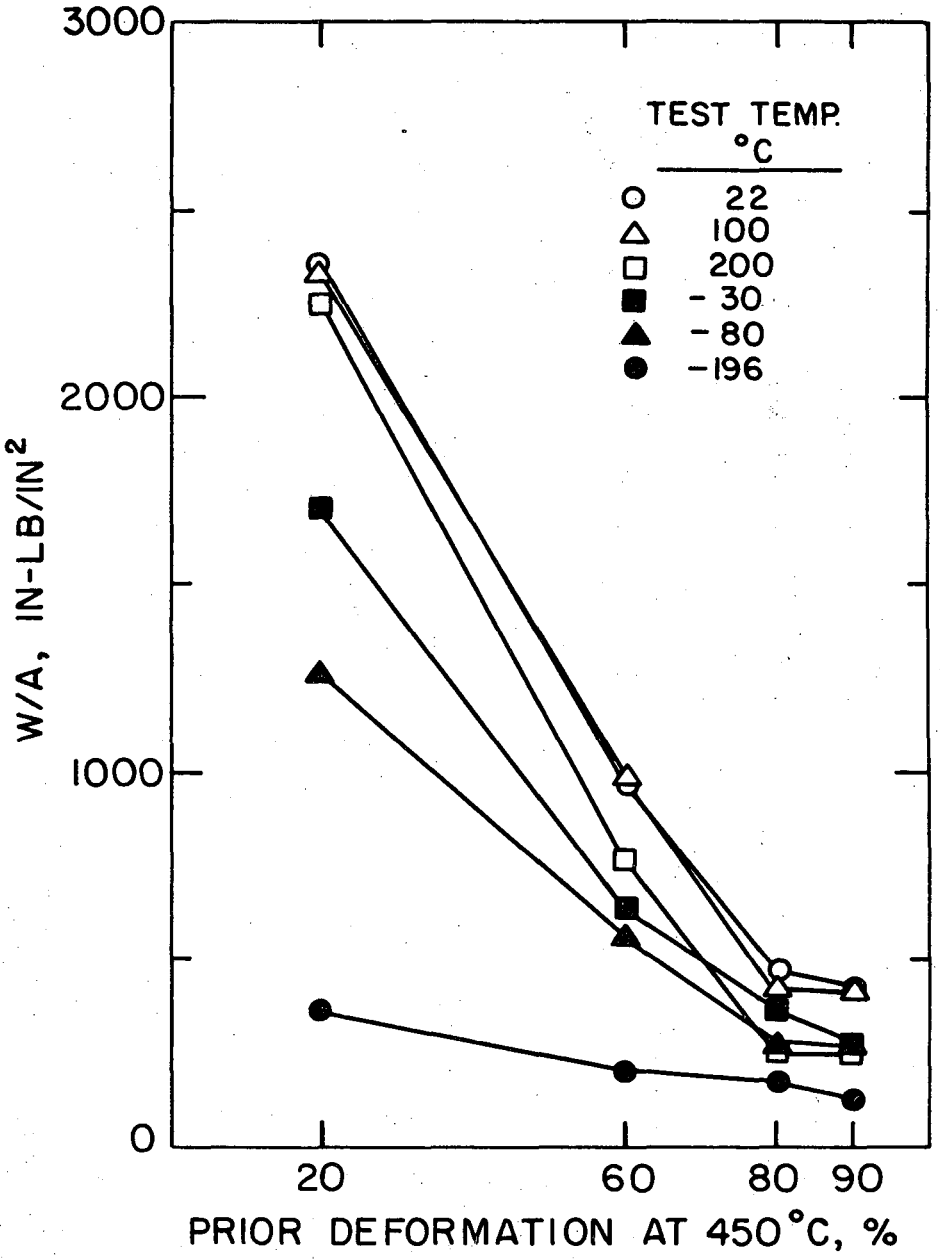

XBL 698-1296

Fig. 11(b)

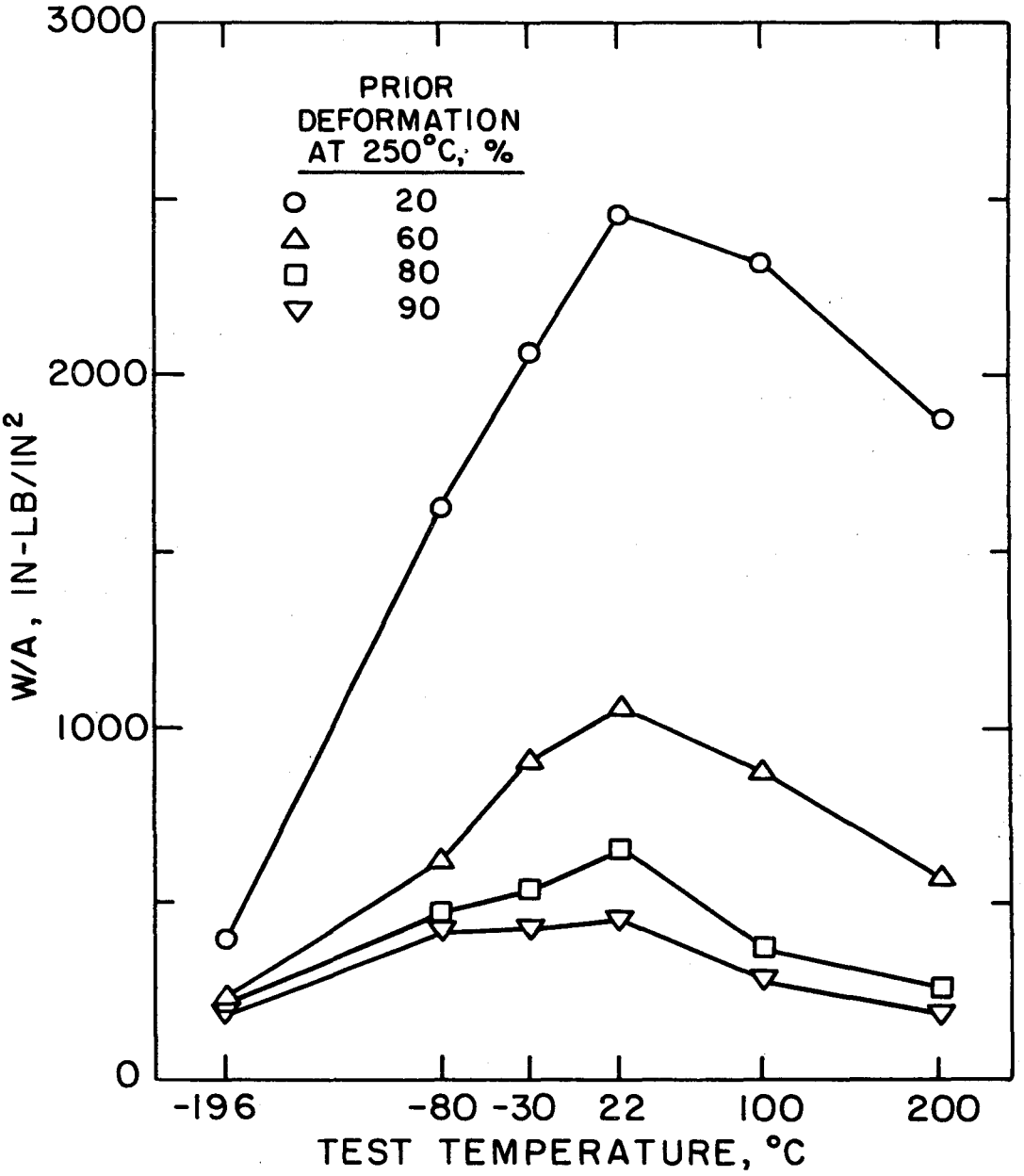
3000
2000
1000
0
W/A, IN-LB/IN²
PRIOR
DEFORMATION
AT 250°C, %
20
60
80
90
-196
-80
-30
22
100
200
TEST TEMPERATURE, °C
XBL 698-1297

Fig. 12(a)

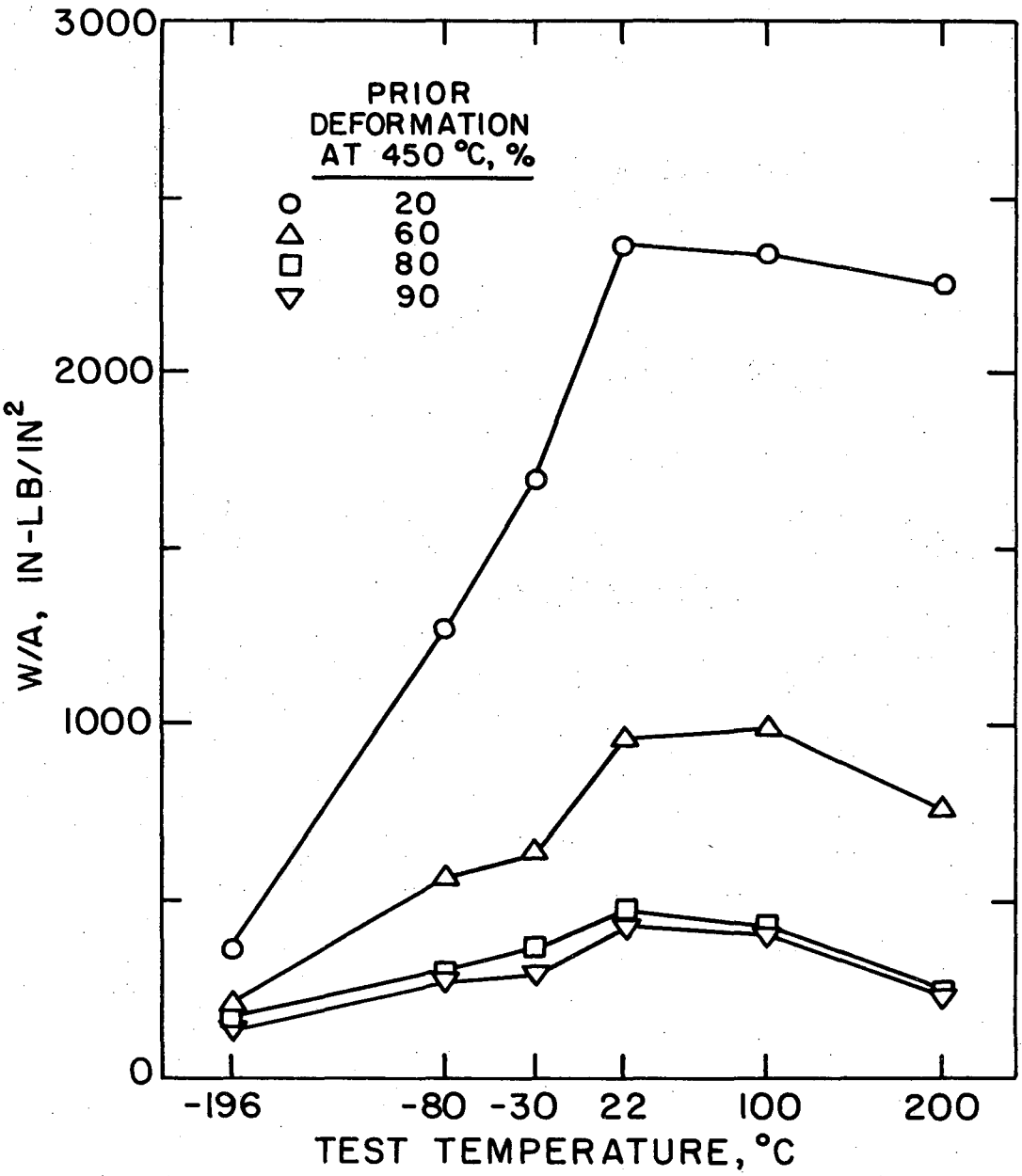
3000
2000
1000
0
W/A, IN-LB/IN²
PRIOR
DEFORMATION
AT 450 °C, %
20
60
80
90
-196
-80
-30
22
100
200
TEST TEMPERATURE, °C
XBL 698-1298

Fig. 12(b)

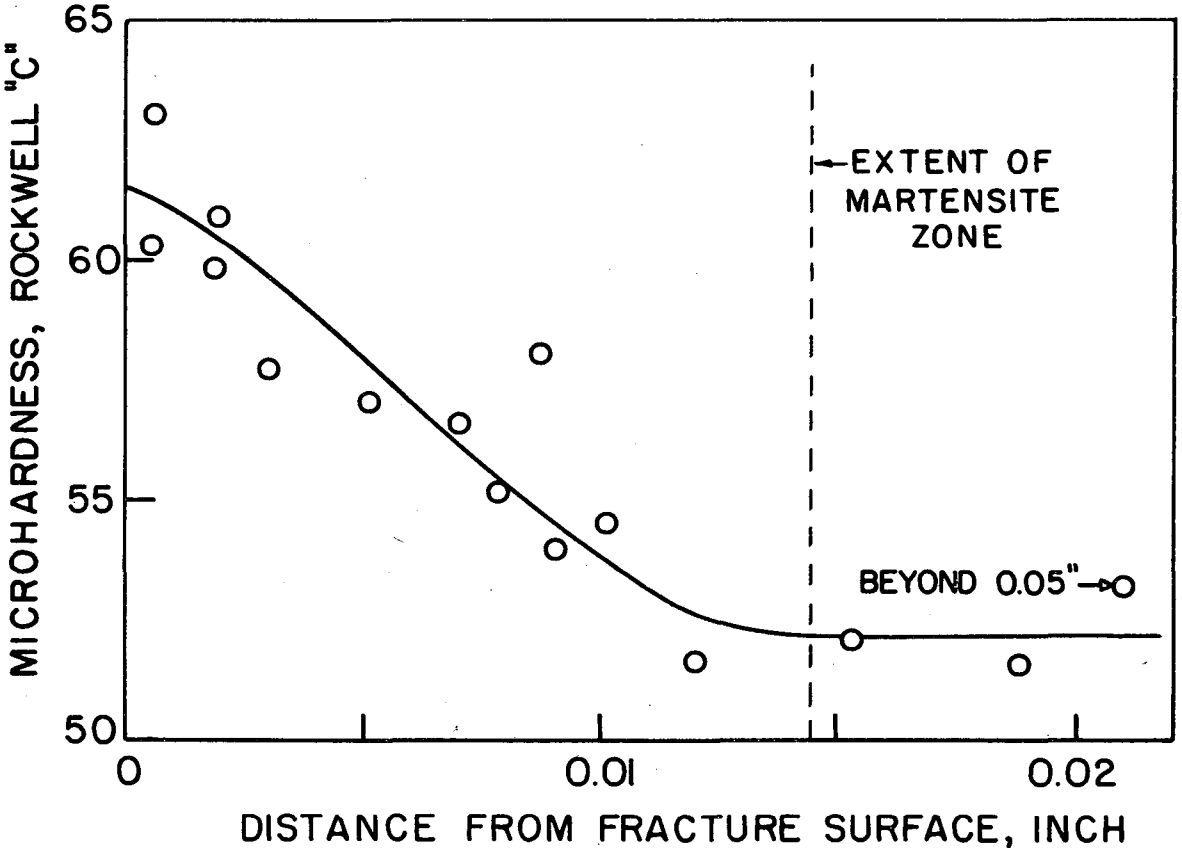

XBL 698-1278

Fig. 13

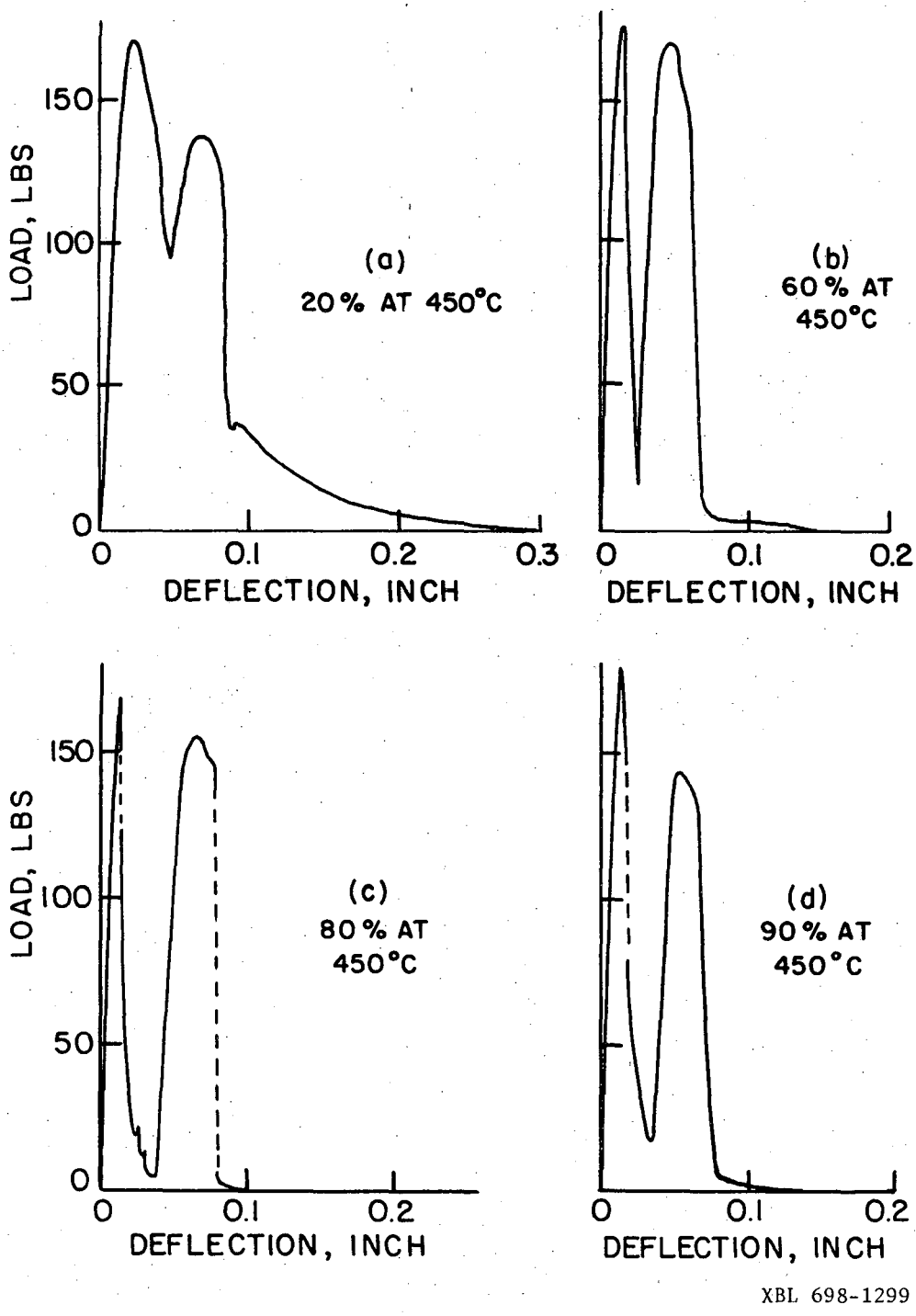
LOAD, LBS
150
100
50
0
(a)
20% AT 450°C
0
0.1
0.2
0.3
DEFLECTION, INCH
(b)
60% AT
450°C
0
0.1
0.2
DEFLECTION, INCH
LOAD, LBS
150
100
50
0
(c)
80% AT
450°C
0
0.1
0.2
DEFLECTION, INCH
(d)
90% AT
450°C
0
0.1
0.2
DEFLECTION, INCH
XBL 698-1299

Fig. 14

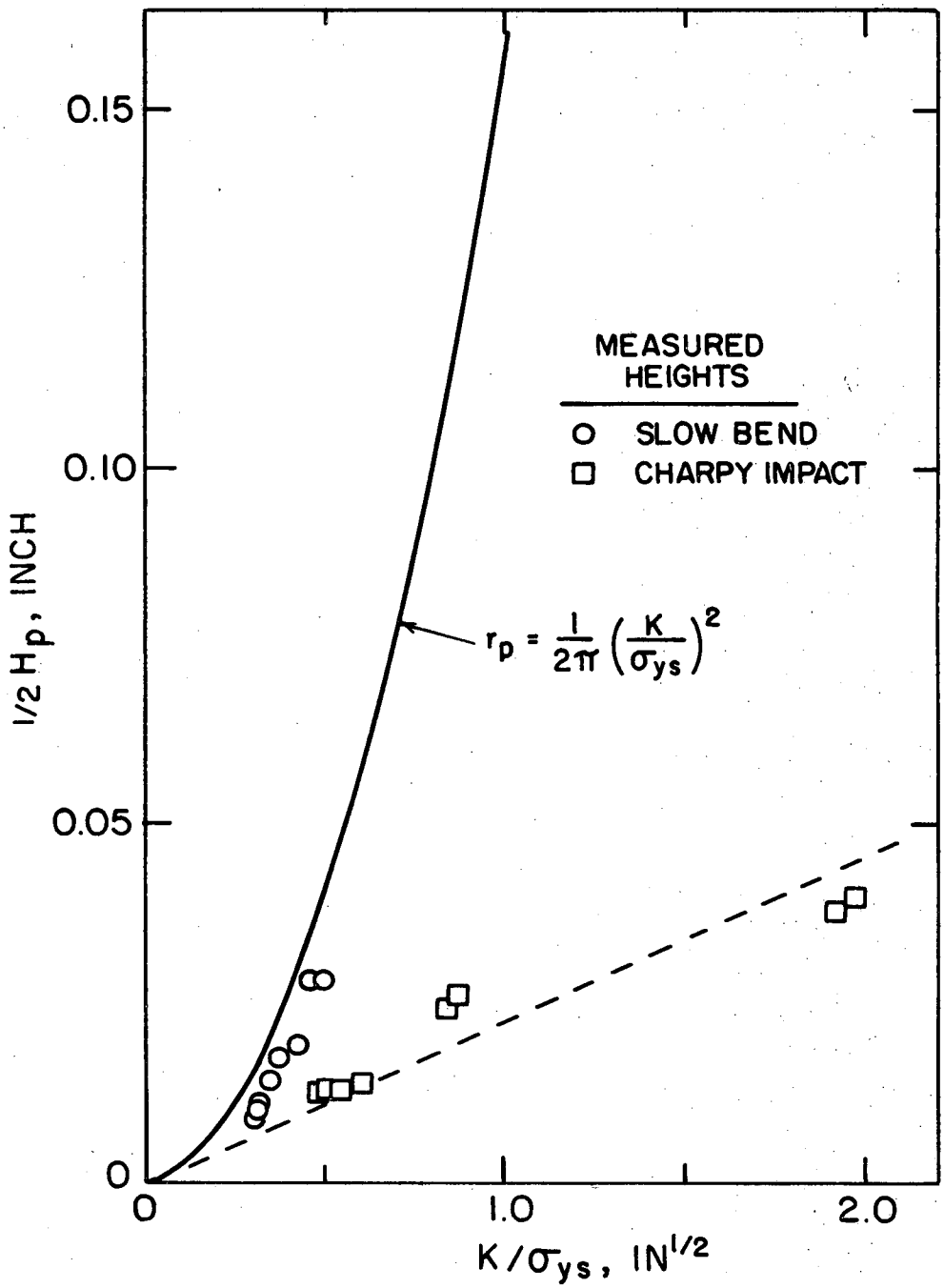

XBL 698-1300

Fig. 15

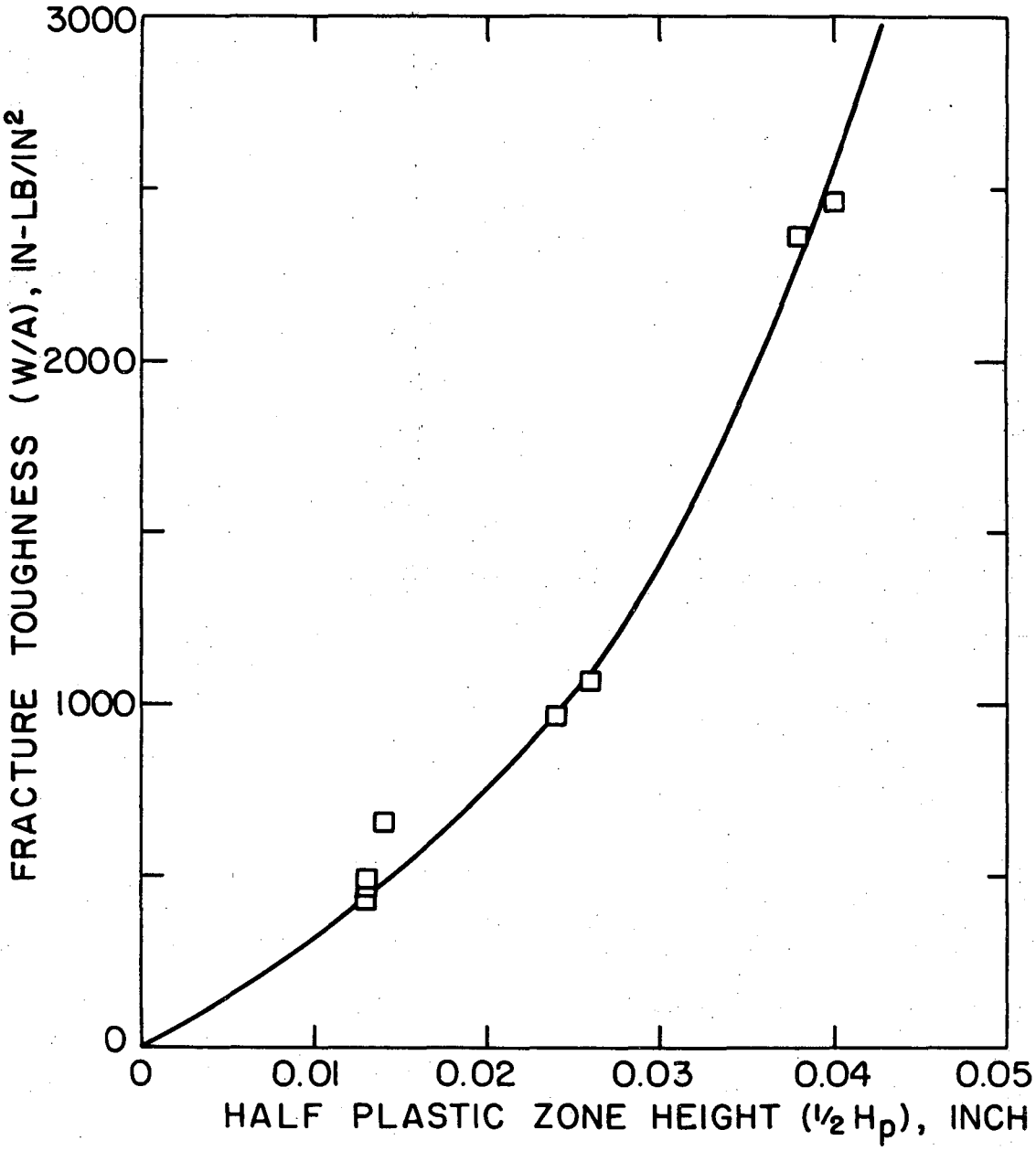

XBL 698-1301

Fig. 16

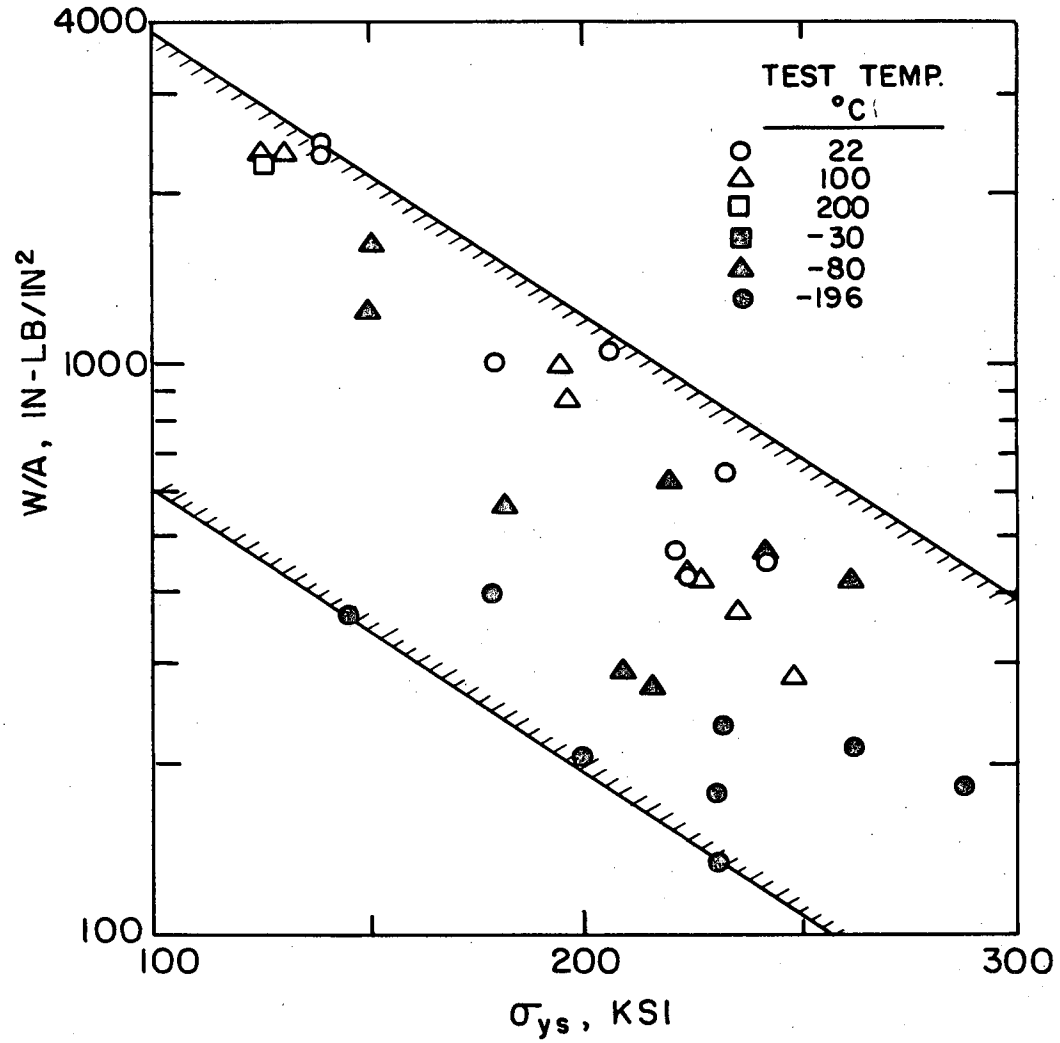

XBL 698-1281

Fig. 17

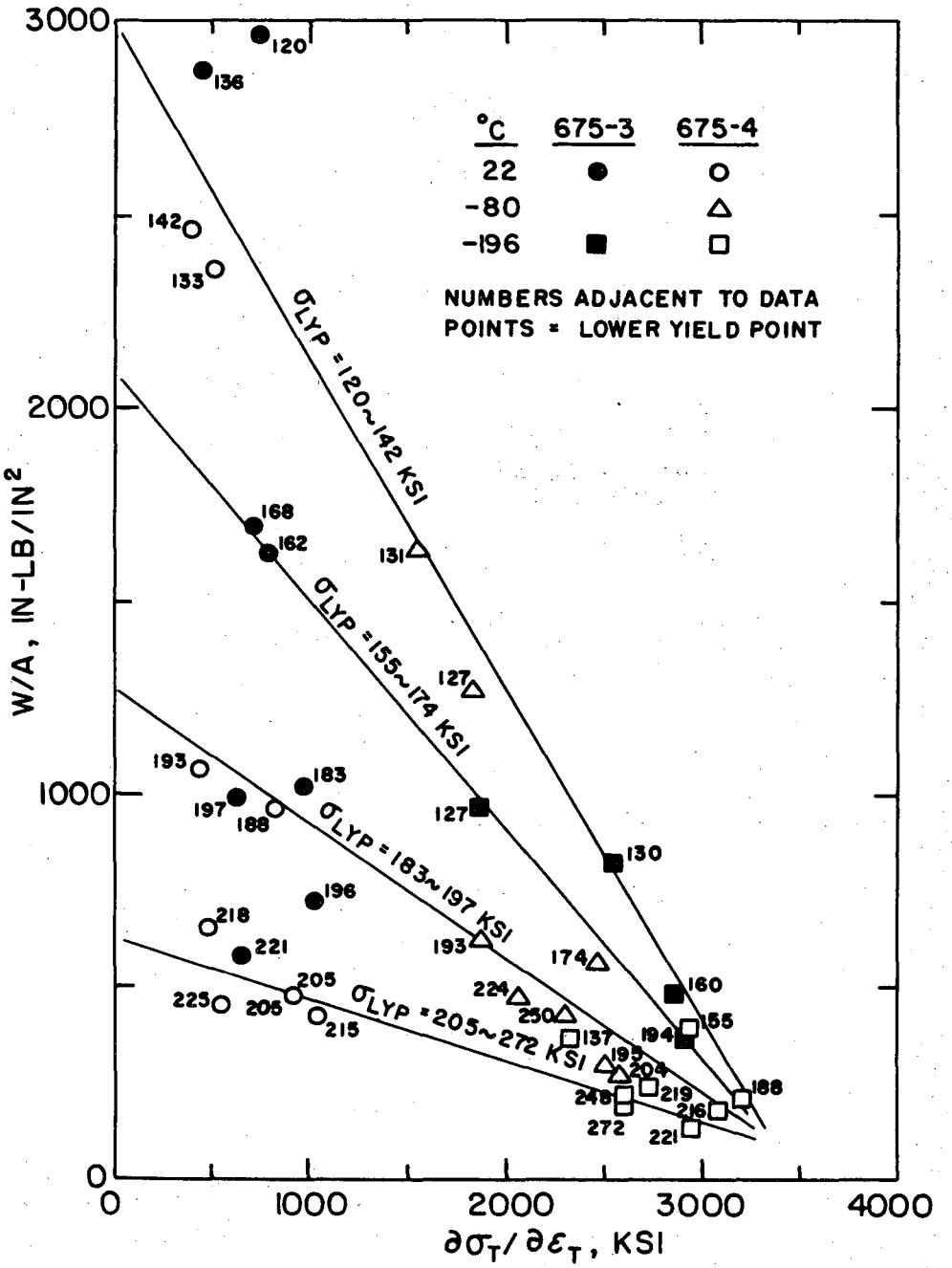

XBL 698-1302

Fig. 18

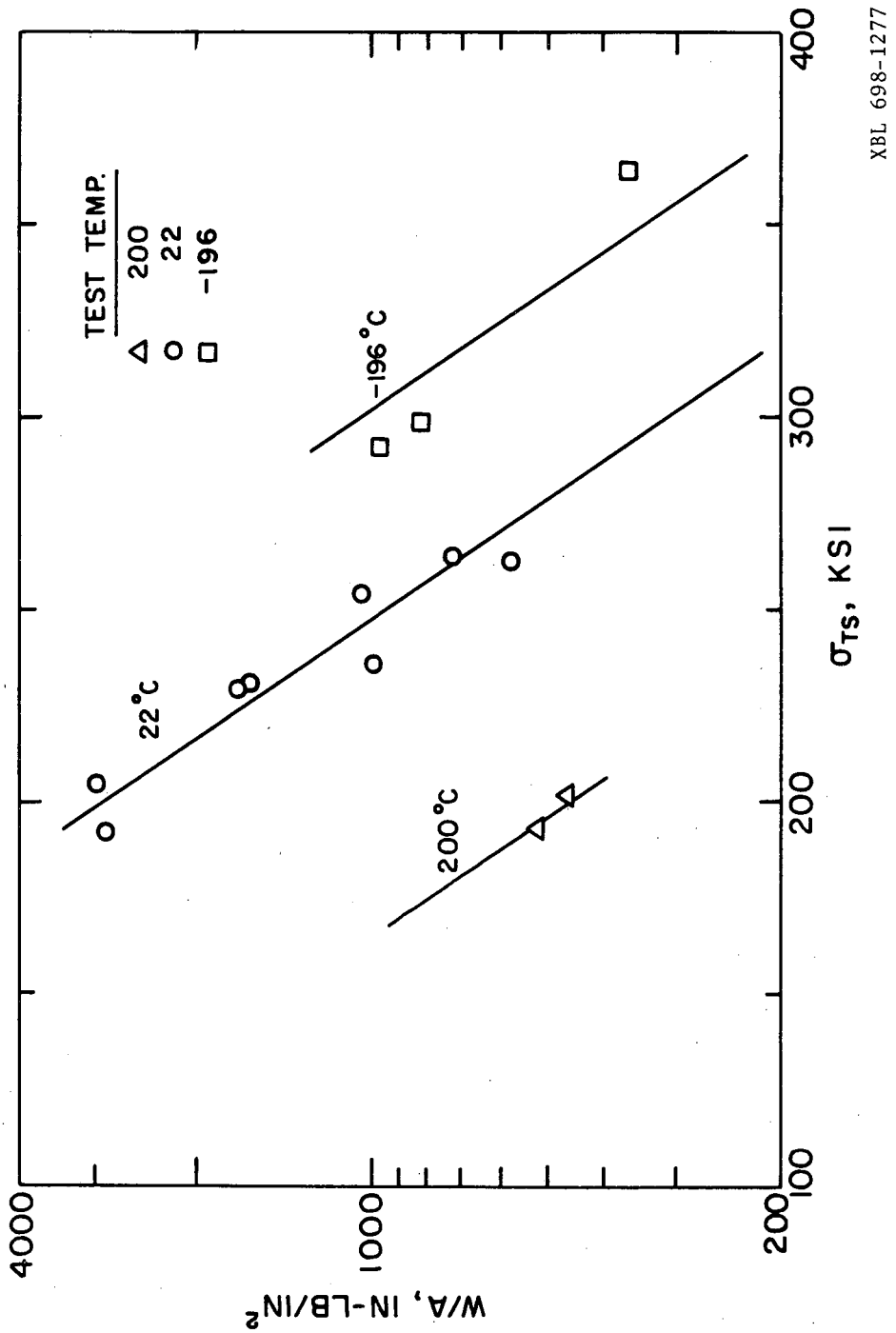
TEST TEMP.
200
22
-196
-196°C
22°C
200°C
W/A, IN-LB/IN²
4000
1000
200
100
200
300
400
σTS, KSI
XBL 698-1277

Fig. 19

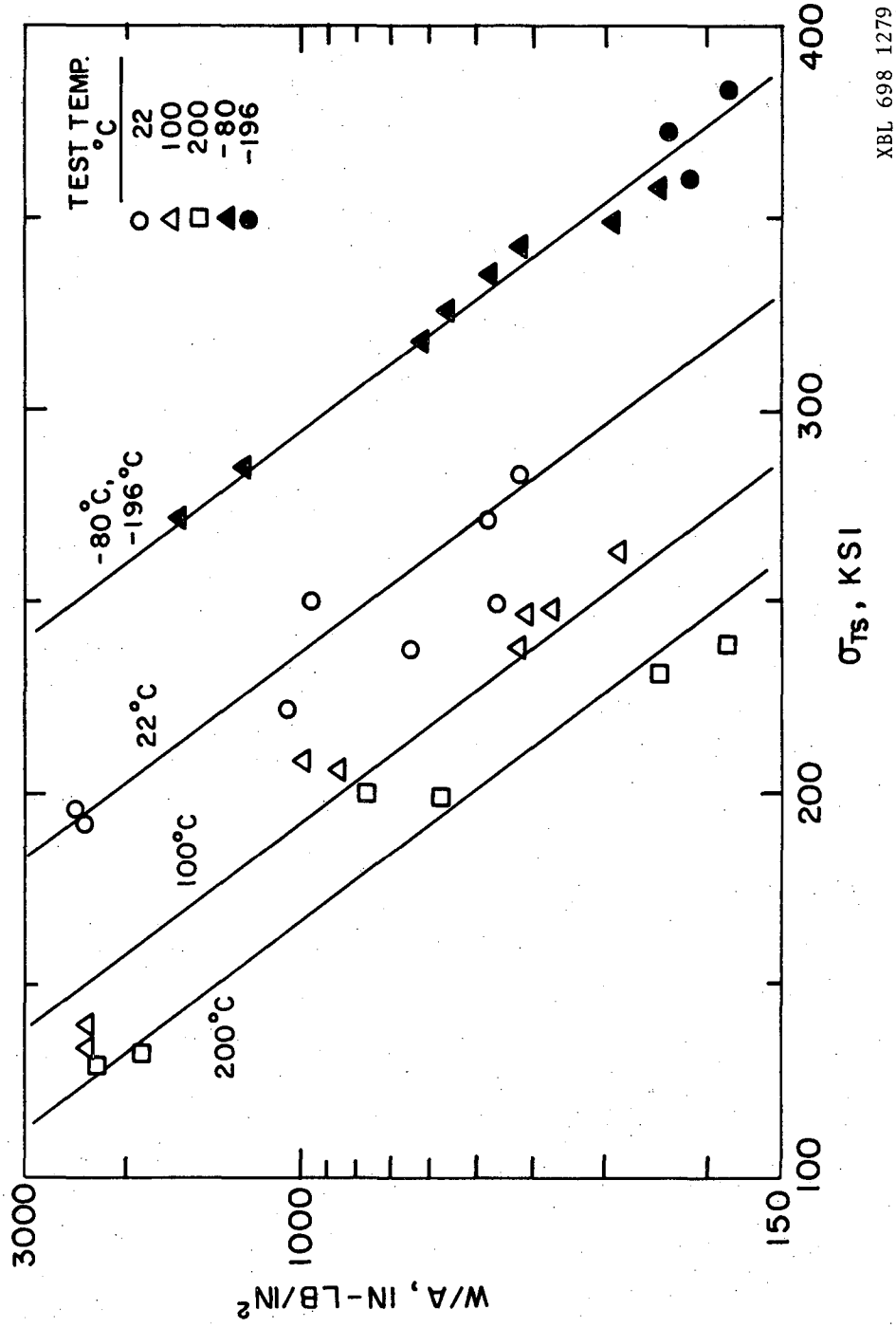
TEST TEMP. °C
22
100
200
-80
-196
-80°C, -196°C
22°C
100°C
200°C
W/A, IN-LB/IN²
3000
1000
150
100
200
300
400
σTS, KSI
XBL 698 1279

Fig. 20(a)

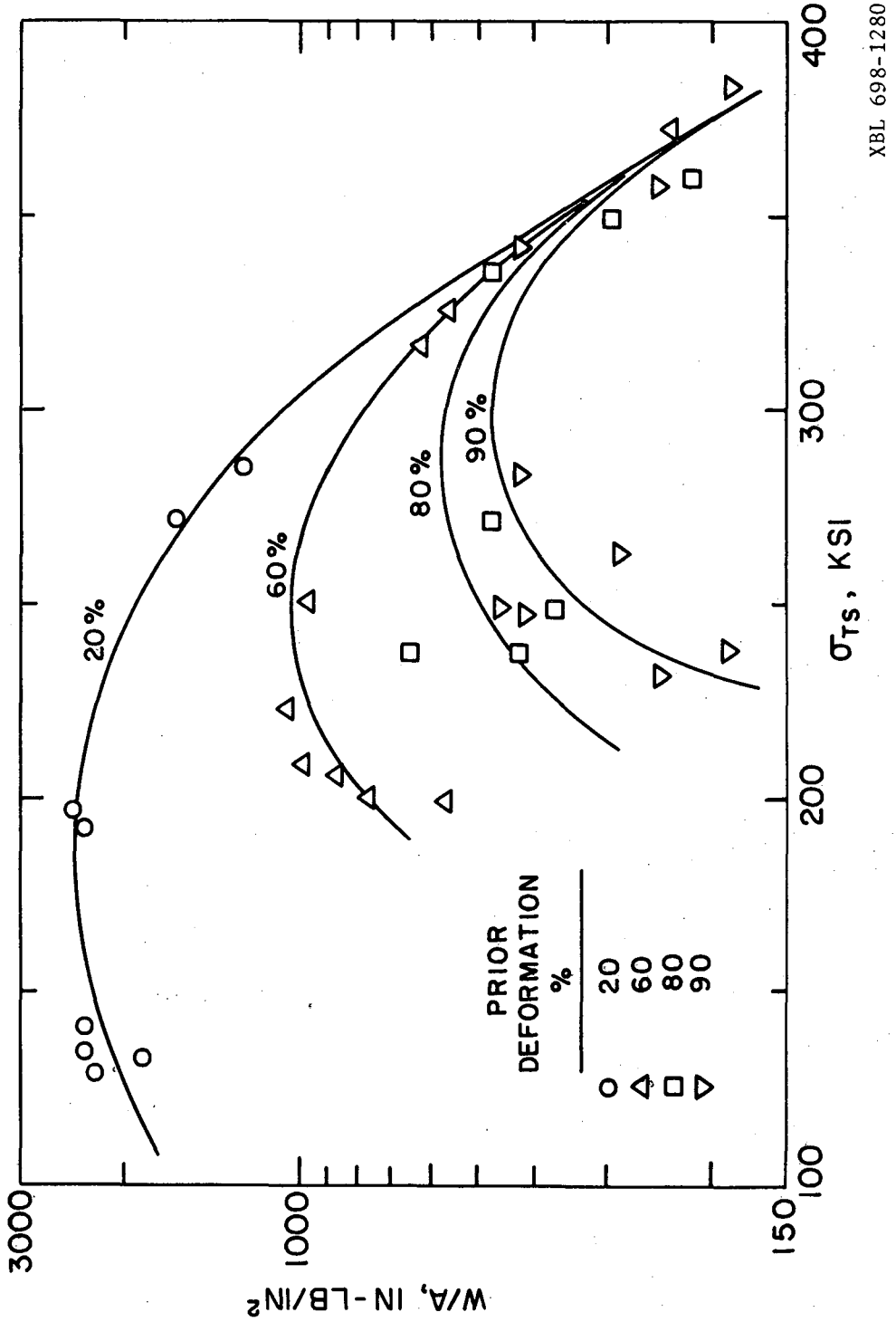

XBL 698-1280

Fig. 20(b)

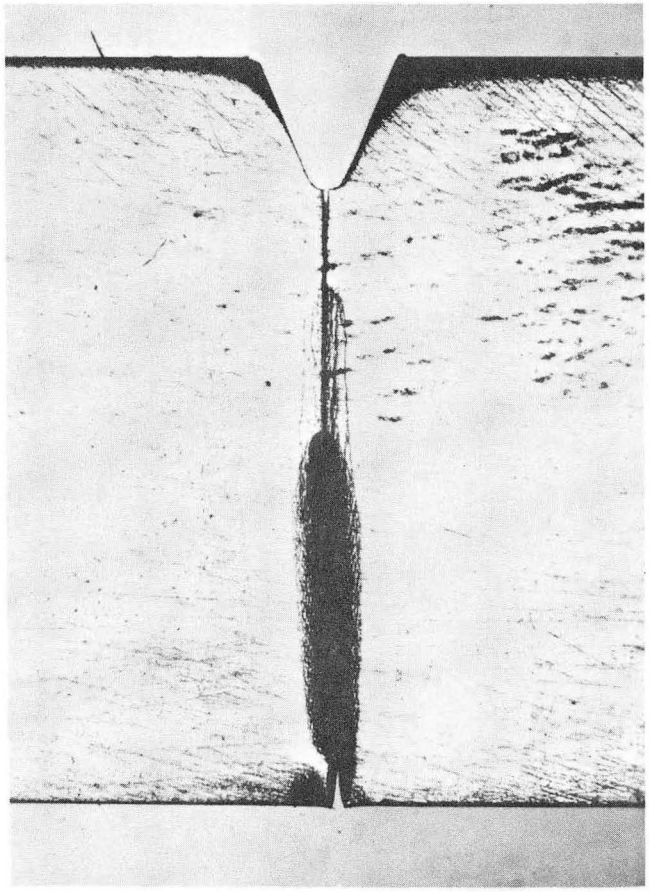

Fig. 21(a)

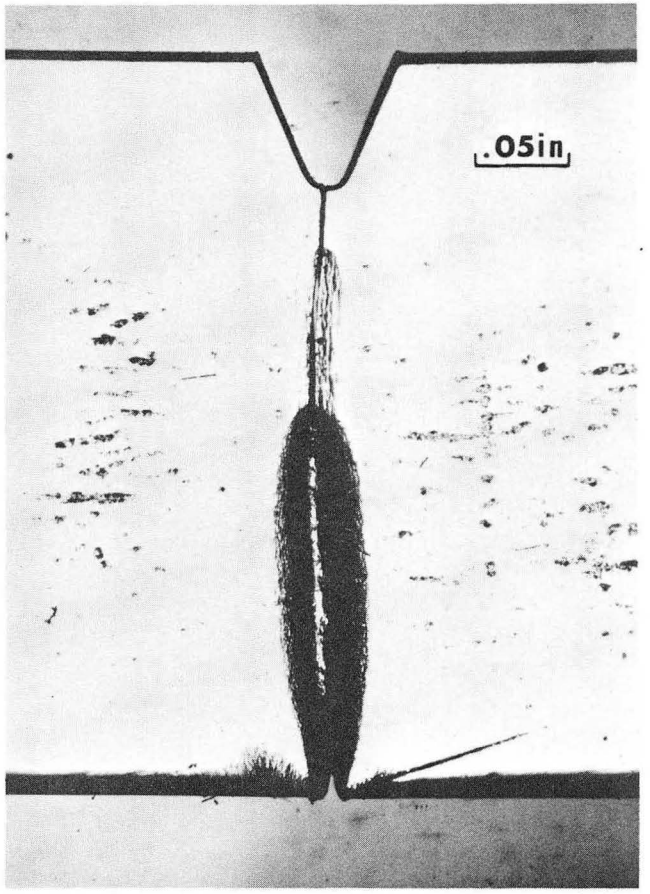

XBB 698-5416

Fig. 21(b)

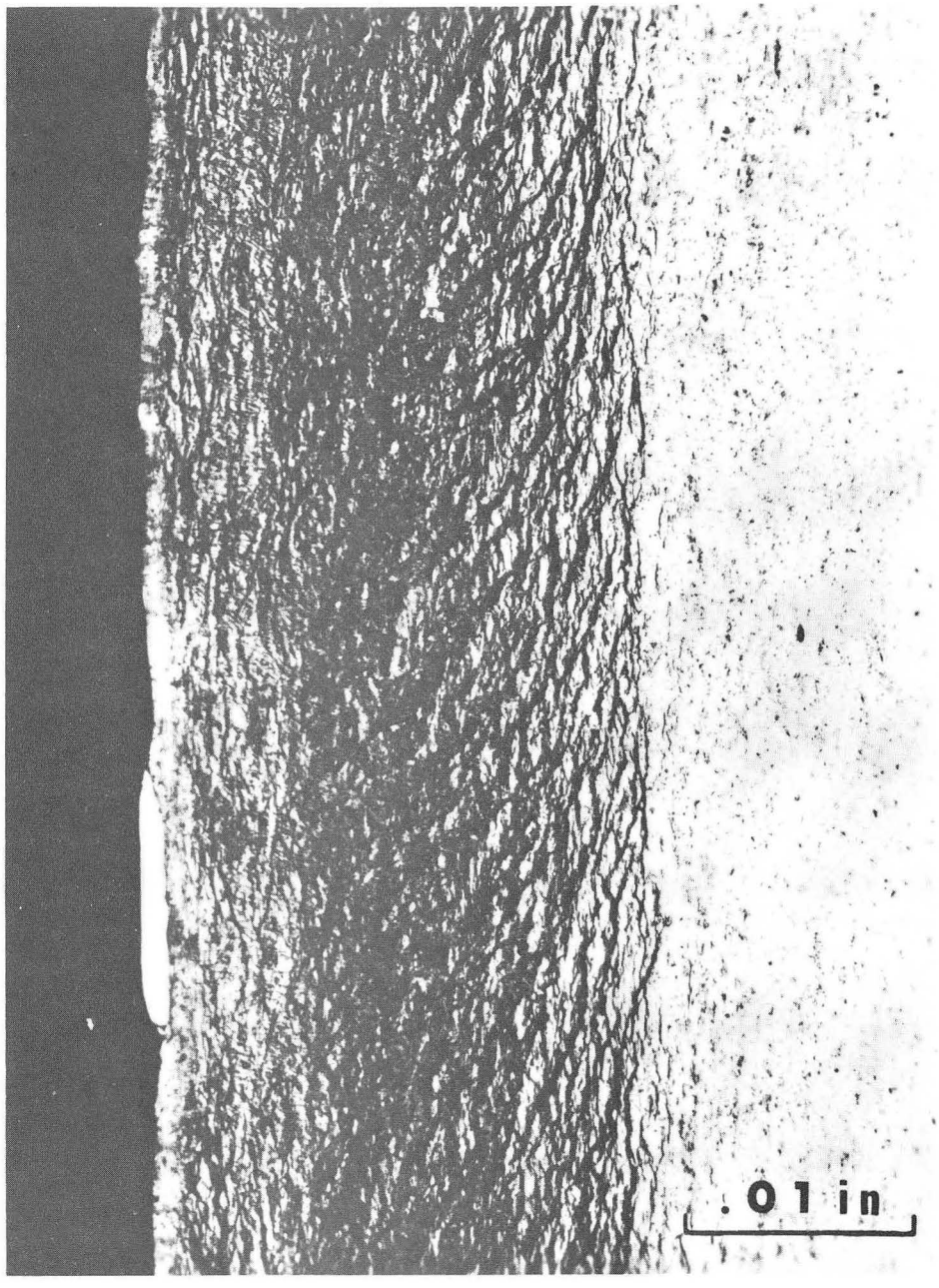

XBB 698-5418

Fig. 22

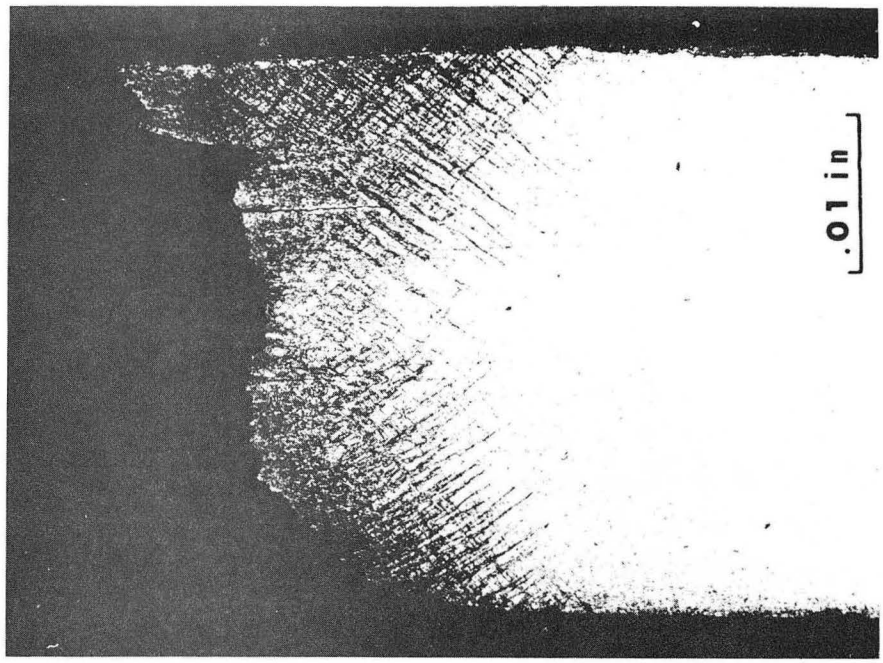

XBB 698-5417

Fig. 23(b)

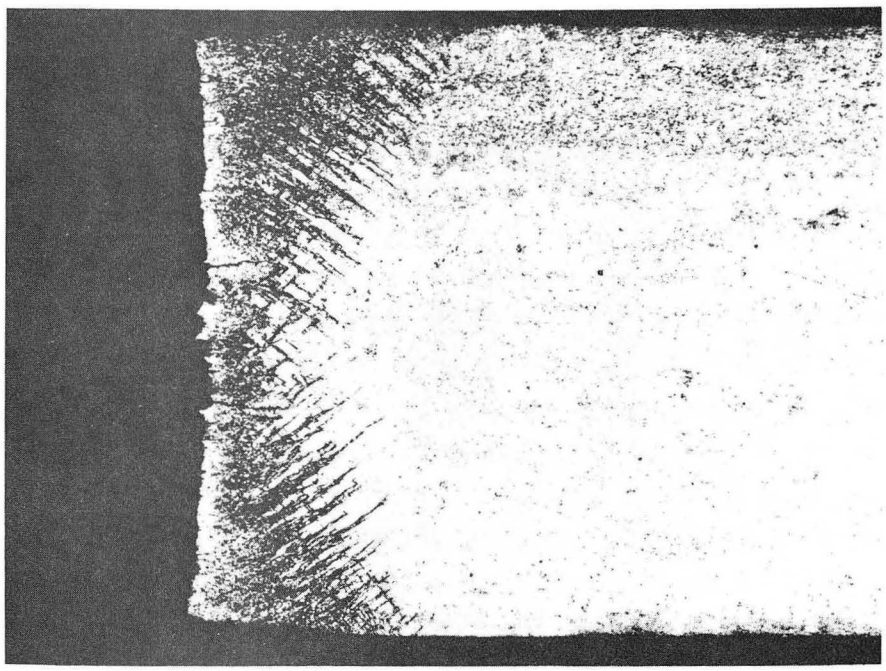

Fig. 23(a)

LEGAL NOTICE

This report was prepared as an account of Government sponsored work. Neither the United States, nor the Commission, nor any person acting on behalf of the Commission:

A. Makes any warranty or representation, expressed or implied, with respect to the accuracy, completeness, or usefulness of the information contained in this report, or that the use of any information, apparatus, method, or process disclosed in this report may not infringe privately owned rights; or

B. Assumes any liabilities with respect to the use of, or for damages resulting from the use of any information, apparatus, method, or process disclosed in this report.

As used in the above, "person acting on behalf of the Commission" includes any employee or contractor of the Commission, or employee of such contractor, to the extent that such employee or contractor of the Commission, or employee of such contractor prepares, disseminates, or provides access to, any information pursuant to his employment or contract with the Commission, or his employment with such contractor.

TECHNICAL INFORMATION DIVISION
LAWRENCE RADIATION LABORATORY
UNIVERSITY OF CALIFORNIA
BERKELEY, CALIFORNIA 94720